REVISION 2

Interaction of methane hydrate complexes with smectites: experimental results compared to molecular models

Rubén Martos-Villa[1], Stephen Guggenheim[2] , M. Pilar Mata[3] , C. Ignacio Sainz-Díaz[4] and Fernando Nieto [4,5]

[1] Facultad de Ciencias del Mar y Ambientales, Universidad de Cádiz, Av. República Saharaui s/n, 11510, Puerto Real, Spain. ruben.martos@uca.es

[2] University of Illinois at Chicago, 845 W. Taylor St., Chicago, Illinois 60607, U. S. A.

[3] Instituto Geológico y Minero de España, Rios Rosas, 23, 28003, Madrid Spain.

[4] Instituto Andaluz de Ciencias de la Tierra, CSIC-Universidad de Granada, Av. De las Palmeras, 4, 18100, Armilla, Granada, Spain.

[5] Universidad de Granada-CSIC, Av. Fuentenueva s/n, 18002, Granada, Spain.

ABSTRACT

Molecular simulations were performed to determine the structure and behavior of methane hydrate complexes in the interlayer of Na-rich montmorillonite and beidellite smectite. Molecular dynamics (MD) simulations used NPT ensembles in a 4x4x1 supercell comprised of montmorillonite or beidellite with methane hydrate complexes in the interlayer. The simulations presented here are in agreement with experimental data that shows a significantly expanded interlayer (Guggenheim and Koster van Groos, 2003; Koster van Groos and Guggenheim, 2009). The smectite 2:1 layer forms part of the coordination sphere enclosing methane molecules; the MD results show that water molecules close to the siloxane surface form mixed cages that enclose methane molecules between basal oxygen atoms of the silicate rings and water molecules from the hydrogen bonding network.

However, the higher tetrahedral charge did not favor the formation of methane hydrate components in the interlayer. Thus, methane hydrate complexes can be formed in pure montmorillonite more easily than in beidellite.

Clay minerals obtained from marine localities with associated methane seeps and with variable Na, K, Ca and Mg interlayer compositions were used to examine how swelling capacity affects the crystallization of smectite-methane-hydrate complexes. Results show that the formation of these complexes is dependent on the swelling capacity in the smectite. In samples with limited swelling properties, methane hydrate is formed in the pore spaces between particles and on the external surface of clays.

INTRODUCTION

Gas storage in nature is one of the most important issues in the last decade because of concern about climate change caused by CO_2 emissions. One related reaction is direct mineral carbonation, but the number of studies relating to gas storage as a hydrate is increasing. A natural laboratory for gas storage is submarine mud volcanoes at continental margins. A mud volcano is generated by extrusion activity involving the transport of clay-rich sediments, liquids and gases (mainly methane) from deeper regions to the seafloor (Milkov, 2000; Kopf, 2002). In gas-hydrate bearing marine sediments, smectite has been described as an abundant clay mineral (Kerr et al., 1970; Robertson and Kopf, 1998; Clennell et al., 1999; Zitter 2004; Martín-Puertas et al., 2007), but the clay mineralogy is complex. In addition, there is a close relation between fluids and the nature of clays, as a result of diagenetic transformations at depth. Smectite illitization occurs at temperature ranges of ~80 to ~150 ºC (Hower et al., 1976; Abid et al., 2004; Aróstegui et al., 2006),

where smectite is transformed to randomly interstratified (R0) illite-smectite minerals (I-S) and to more illitic ordered (R1-R3) I-S (Hower et al., 1976; Velde and Vasseur, 1992).

Clay-rich rocks can incorporate considerable amounts of methane (Ertefai et al., 2010; Hinrichs et al., 2006). Methane may be stored in the pores of the clay rock as free-gas and adsorbed onto the surfaces of clay minerals (Ji et al., 2012, Zhang et al., 2012). The amount of methane adsorbed on clay surfaces represents a major component of shale gas, an unconventional gas resource. The gas sorption capacity is affected by the clay mineral composition and the microporosity (Aringhieri, 2004; Wang et al., 2004).

Swelling clays, such as montmorillonite and beidellite, usually contain multiple planes of weakly bonded H_2O in the interlayer between the 2:1 (silicate) layers. The weakness of the atomic interactions between H_2O molecules and the 2:1 layer, and the fact that the interlayer region is adjacent to two surfaces suggest that adsorption processes occur in the interlayer.

Gas hydrates, including methane hydrates, are crystalline compounds consisting of gas molecules in cavities within a hydrogen-bonded network of water molecules. Methane hydrates may occur as a cubic sI structure that consists of 46 water molecules per unit cell, forming two dodecahedron (5^{12}) and six tetradecahedron ($5^{12}6^2$) cages (Sloan, 1998). Medium pressures (> 20 Bar), low temperatures (273-290 K) and a high methane gas concentration in water ($X_{CH4} \sim 0.0015$) are required to form methane hydrates (Henry et al., 1999; Jager and Sloan, 2001; Davie et al., 2004; Sun and Duan, 2007). These conditions can occur naturally in permafrost and in sediments of the ocean floor along the outer continental margin (Kvenvolden, 1998; Buffet, 2000; Milkov, 2005) where fine-grained sediments exist. A better understanding of the molecular interactions leading to hydrate crystallization and

decomposition is crucial because destabilization of methane hydrates may play an important role in climate change (Archer, 2007).

In the solar system, methane hydrate is considered to be one of the major constituents of the outer planets such as Neptune and Uranus and their moons, such as Titan (Machida et al., 2006). Indeed, silicates are also an ubiquitous material throughout the Universe and they are present in interplanetary dust and in the planets and moons; for example, clays has been detected on Mars (Ehlmann et al., 2008; Wray and Ehlmann, 2011). Methane in the Martian atmosphere has been recently detected (Gough et al., 2010) and perhaps methane is released to the Martian atmosphere from decomposition of subsurface clathrate layers (Chastain and Chevrier, 2007, Chassefiére, 2009).

Theoretical studies involving computational mineralogy may be very useful to understand and interpret experimental results. Molecular calculations on the structural and thermodynamic properties of gas hydrates have been performed by means of Density Functional Theory (DFT) (Du et al., 2008). Ab initio quantum mechanical methods (Klauda and Sandler, 2002; Sun and Duan, 2007), using cluster models and crystal lattice models, have been used to describe the weak guest-host interactions in hydrates. Molecular Dynamic (MD) simulations involving several force fields were used to calculate the crystal structure (Chihaia et al., 2005; Rodger, 1990) and to describe different properties of methane hydrates, including mechanisms of nucleation and crystal-growth kinetics (Conde et al., 2010; Liang and Kusalik, 2010; Zhang and Pan, 2011), mechanisms of decomposition (Bagherzadeh et al., 2012; Myshakin et al., 2009), and inhibition mechanisms of hydrate formation (Anderson et al., 2005).

Because of the swelling- and exchange-capacity of many clays, several experimental and theoretical studies have focused on the interaction of hydrates and 2:1 clays. Cha et al. (1988) showed the importance of large specific surface areas in the nucleation of gas hydrates, demonstrating that methane hydrates in bentonites are more stable than in water alone. Guggenheim and Koster van Groos (2003) and Koster van Groos and Guggenheim (2009) succeeded in intercalating methane hydrate complexes between the 2:1 layers of Na-exchanged montmorillonite. These authors highlighted the potential importance, not considered so far, of gas trapping by clay minerals in marine environments. In this scenario, the swelling properties of clays are controlled by ocean-floor pressures and temperatures, sea-salt content, and types of clay minerals. Experimental data with natural samples are necessary to determine if the methane hydrate complexes can intercalate in the expected variety of clays present at the sea-floor and particularly in gas hydrate reservoirs and mud volcanoes.

Because of the limited experimental data and analyses of natural samples, molecular modeling has been used to obtain information about the intercalation of methane in smectites. Park and Sposito (2003) and Titiloye and Skipper (2000, 2001) performed Monte Carlo and MD simulations by introducing a mixture of methane and H_2O in the interlayer as an initial model. After simulations, they found that each methane molecule was solvated by 12-13 H_2O molecules and 8 oxygen atoms of the tetrahedral sheet at the 2:1 layer surface to form a coordination shell in an amorphous hydrate structure in the interlayer. Also, Zhou et al. (2011) studied the effect of layer charge on the hydration of methane intercalated in Na-smectite models. They obtained a disordered hydrate-like coordination structure and they found that the hydrate complex is more stable in smectites with the layer charge dominated by tetrahedral cations.

Cygan et al. (2004) performed MD simulations based on interatomic potentials on a model with a cluster composed of one unit cell of methane hydrate included in a 3 x 2 x 1 Na-montmorillonite supercell. Their results showed a *d*-value of the intercalate close to that obtained in experiments by Guggenheim and Koster van Groos (2003). In the present paper, a 4 x 4 x 1 smectite supercell (10 unit cells larger than previous models), with the methane hydrate complex occupying all the interlayer space, not just a small methane hydrate cluster, is modeled thereby allowing the methane hydrate complex in the interlayer to maintain periodicity. Also, different layer charges are compared by modeling montmorillonite and beidellite smectites, thereby examining a greater number of smectite compositions.

The purpose of this work is to determine the behavior at an atomistic level of methane hydrate complexes in an expanded clay-mineral structure model by molecular simulations. One goal is to determine how clay-rich methane-bearing marine sediments react with methane by applying the experimental aproach of Guggenheim and Koster van Groos (2003) and Koster van Groos and Guggenheim (2009). An additional goal is to understand how layer charge affects the formation of smectite-hydrate complexes by using molecular models. Theoretical data demonstrate that subtle differences involving how the origin of the layer charge (i.e. tetrahedral vs octahedral cation substitutions) can affect the formation of methane hydrate complexes in the interlayer. Molecular simulations can also describe the behavior of these intercalates.

Experimental Methodology

Five clay-rich samples (A2, M3, M4, M8 and M12) were selected from short gravity cores of mud volcanoes from the Gulf of Cádiz area (León et al., 2012; Somoza et al., 2003).

144 X-ray diffraction (XRD) patterns of bulk samples with a size fraction of <2 μm were
145 obtained using a Bruker D8 Advance diffractometer, located at The University of Cádiz,
146 with a graphite monochromator, operating at 40 kV and 40 mA using Cu-Kα radiation. Each
147 sample was first washed with distilled water until the supernatant was chloride-free,
148 sonicated and then the <2 μm fraction was separated by centrifugation. Each suspension was
149 smeared on glass slides and air dried in atmospheric conditions. The slides were then
150 saturated with ethylene glycol at 80 ºC for 24 h to ensure maximum saturation.
151
152 Grain morphology within the bulk and the <2 μm fractions, and quantitative chemical
153 analyses by analytical electron microscopy (AEM) were obtained by using a Philips CM20
154 transmission electron microscope (TEM). Powdered portions deposited on a holey C-coated
155 Au grid were used to collect AEM spectra in scanning transmission electron microscopy
156 (STEM) mode on areas of 200 x 1000 Å using a 70 Å diameter spot size. To check
157 volatilization of light elements, analyses were taken at 15 and 40 s. The structural formulae
158 of smectites, micas and interstratified I-S were calculated on the basis of 22 negative
159 charges, i.e. $O_{10}(OH)_2$, adjusting the occupation of the octahedral sheet to 2 atoms per
160 formula unit.
161
162 A powder X-ray diffraction environmental chamber designed by Koster van Groos et al.
163 (2003) was used to analyze *in situ* hydrates and smectite-methane hydrate complexes. The
164 environmental chamber allows pressures of <70 bar and temperatures from -50 to 100 ºC.
165 The chamber is mounted on a Siemens Theta-Theta powder X-ray diffractometer, model D-
166 5000. The operating conditions were 45 kV and 25 mA, using Cu Kα radiation and a
167 graphite monochromator equipped with a Peltier-cooled, solid-state detector. Temperature

168 was controlled using a Neslab RTE-111 refrigerating bath/circulation unit, precise to within
169 0.1ºC, using an alcohol refrigerant. A K-type thermocouple, located at 2 mm to the sample,
170 was used to monitor temperature. In all experiments, bottled research-grade CH_4 gas was
171 used. Pressure was measured with a calibrated digital Heise pressure gauge that is
172 considered to be accurate to within 0.2%. The glass slide, located at the chamber center in
173 reflecting position, was coated with an extremely thin film of clay (~300 nm) suspension to
174 form a thin, oriented aggregate. The chamber was maintained at high moisture conditions
175 until the (001) peak was greater than 36 Å (ie., at 2θ values of <2º). Then, the chamber was
176 sealed and methane gas was pumped into the chamber until the desired *P*-*T* conditions were
177 obtained. The sample was analyzed by periodical scans using XRD.
178
179 **Computational Methodology**
180 The molecular electronic structure of isolated molecules and hydrated sodium ions
181 was studied by quantum chemical calculations with the Hartree-Fock approximation and the
182 second-order Moeller-Plesset method for all electrons. A triple-ζ basis set with polarization
183 functions was used for all atoms including H atoms (MP2/6-311G** level) as implemented
184 in the Gaussian03 program package (Frisch et al., 2004). All geometries were fully
185 optimized using the Berny analytical gradient method. No geometry constraint was applied
186 to the molecules. Normal mode analyses were performed to the same level to confirm the
187 nature of the various stationary points, finding only positive eigenvalues for minima.
188 Because quantum mechanical methods do not describe the dispersive interactions and
189 weak adsorption interactions well, empirical interatomic potentials were used. These
190 empirical potentials were used within a Force Field (FF) that has recently been optimized by
191 Heinz et al. (2005) based on CVFF (consistent valence force field) and this method has been

named CVFFH. The CVFFH method yielded good results in phyllosilicates with organic molecules (Sainz-Díaz et al., 2011). The atomic charges were taken from charges calculated at the ab initio MP2/6-311G** level and associated with the electrostatic field (ESP) with the method of Merz and Kollman (Besler et al., 1990) for the methane molecule. Different calculation conditions were tuned with respect to the 12-6 (CVFF) Lennard-Jones potentials and with van der Waals and Coulomb interactions. The van der Waals atom based interactions with a cut-off of 15.5 Å and the Ewald summation for Coulomb interactions yielded the best results, and these conditions were used in this work. Molecular dynamic simulations were performed with this force field with several ensembles and steps of 1 fs. The temperature and pressure of the model system were controlled using Andersen (Andersen, 1980) and Berendsen (Berendsen et al., 1984) methods, respectively. For these CVFFH calculations, periodical boundary conditions for crystal lattice structures with the Discover program within the Material Studio package (Accelrys, 2009) were used.

In all cases, the adsorption energy was calculated from: $U_{adsorption} = U_{smectite\text{-}methane\ hydrate\ intercalate} - (U_{methane\ hydrate} + U_{smectite})$, where U is the internal energy of the system.

Models

Montmorillonite and beidellite models were based on previous pyrophyllite models (Molina-Montes et al., 2008). Pyrophyllite is a dioctahedral phyllosilicate (Lee and Guggenheim, 1981) with a structure similar to montmorillonite and beidellite, but without cation substitutions and layer charge. To obtain a reasonable size model, a 4 x 4 x 1 supercell was created. For the montmorillonite model, ten Al^{3+} are replaced by Mg^{2+} and layer charge is balanced by ten tetrahedrally hydrated Na^{+} cations in the interlayer, resulting in a simulation cell composition of $[Na_{10}][Al_{54}Mg_{10}][Si_{128}]O_{320}(OH)_{64}\ 40H_2O$ (Fig. 1a). The

beidellite model was created by replacing ten tetrahedrally coordinated Si^{4+} by Al^{3+} (5 in each tetrahedral sheet), balancing the charge with ten tetrahedrally hydrated Na^{+} interlayer cations. The beidellite simulation cell has a composition of $[Na_{10}]$ $[Al_{64}][Si_{118}Al_{10}]O_{320}(OH)_{64}$ $40H_2O$ (Fig. 1b). In both cases, maximum dispersion of the substituted cations in the tetrahedral and octahedral sheets was made according to previous studies (Sainz-Díaz et al., 2003, Hernández-Laguna et al., 2006). Initial lattice parameters of each 4 x 4 x 1 smectite supercell are a = 20.64 Å, b = 35.86 Å, c = 12.34 Å; α = 88º, β = 103º, γ = 90º. For smectite-hydrate intercalate models, the c-axis value was set at 30 Å to create sufficient space to introduce unit cells of methane hydrate.

For the hydrated Na^{+} cations, two models were created to agree with previous theoretical calculations (Molina-Montes et al., 2008), consisting of a Na^{+} ion surrounded by four water molecules (tetrahedrally coordinated) and a Na^{+} ion surrounded by six water molecules (octahedrally hydrated). Those models were optimized at the MP2/6-311G** level, keeping a net charge of +1 in the system. The d(Na…O) distances are 2.34 Å and 2.45 Å for tetrahedrally and octahedrally (6-fold) coordinated Na hydrates, respectively (Figure 2). Previous calculations in a 4 x 2 x 1 montmorillonite model showed that the cubic hydrated Na^{+} in the interlayer of montmorillonite has greater dispersion of coordinating water molecules, and montmorillonite lattice parameters are slightly distorted. However, when introducing tetrahedrally hydrated Na^{+} in the interlayer, coordinating water molecules form a plane parallel to the (001). Tetrahedrally hydrated forms produce montmorillonite lattice parameters closer to experimental values at a = 5.16 Å; b = 8.95 Å; c = 12.08 Å; α = 88º; β = 103.3º; γ = 90.1º.

A model of a methane hydrate structure was derived from experimental crystallographic data (Klapproth., 2002). A unit cell was generated including 178 atoms with

240 46 water molecules and 8 methane molecules, with lattice parameters of $a = b = c = 11.97$
241 Å; $\alpha = \beta = \gamma = 90^{\circ}$. Larger simulation cells required for the bulk hydrate structure were
242 created by expanding the unit cell in integral units.

243 For smectite-methane-hydrate intercalate simulations, a 3 x 3 x 1 methane hydrate
244 supercell (414 water molecules + 72 methane molecules) was created with dimensions of
245 20.64 x 35.86 Å. Thus, the hydrate fit into the interlayer of the smectite without losing
246 periodic boundary conditions.

247

248 RESULTS

249 **Experiments**

250 *Clay mineralogy*

251 Bulk mineralogy of samples was analyzed by XRD. Semiquantitative values of XRD are
252 based on peak intensities following the standard procedures using a normalized RIR
253 (Reference Intensity Ratio) method (Chung, 1974a,b, 1975). Bulk mineralogy is comprised
254 of 57-66% of clays in all samples, except for M3 (22%). The major clay-mineral
255 components are smectite, illite-smectite and illite, with minor chlorite, kaolinite and
256 sporadic palygorskite. Carbonates are also abundant, mainly in M3 (6% aragonite and 25%
257 calcite) and are absent in M12. Quartz and feldspar are common (from 17-38%) in all the
258 samples and pyrite is present (<5%) in sample M3.

259

260 XRD and TEM analyses of samples were performed to characterize the clay minerals that
261 might react with the methane + H_2O in the environmental XRD chamber. Although
262 preliminary XRD data indicated that samples were mainly smectite (Martín-Puertas et al.,
263 2007), the deconvolution (using MacDiff 4.2.6) of the pattern obtained from the oriented

mount after glycolation showed that detrital smectite and mixed-layer I-S phases are present in addition to smectite (Mata et al., 2012). A detailed TEM study combining chemistry and the imagery of clay-mineral particles showed morphological differences between the smectite and I-S: smectite, displayed typical aggregates and flakes of irregular and wavy outlines; and I-S showed individual crystals with more euhedral shapes and clear outlines (Figure 3). These morphologies are consistent with TEM observations on smectite illitization by Ferrage et al. (2011). Kaolin hexagonal particles and palygorskite fibers were also present in the samples (Fig. 3, 4, Table 1). Energy-dispersive X-ray spectroscopy (EDS) analysis showed montmorillonite compositions with Mg and K as the interlayer cation, and low tetrahedral charge. Mixed layer I-S chemical analysis revealed an increase in tetrahedral Al and K interlayer content with respect to smectite.

XRD Environmental Chamber

The stability of methane-hydrate intercalates in clays was reported previously for pure smectites (Koster van Groos and Guggenheim, 2009). Those results showed that the 2:1 smectite interlayer accommodated $CH_4 + H_2O$ and stabilized methane-hydrate complexes. Thus, the value of $d(001)$ is dependent on the amount of H_2O present in the interlayer, and a ~22 Å spacing may exist if H_2O is present or if $H_2O + CH_4$ is present, in addition to the exchangeable cations. The 22-Å reflection is not diagnostic for $H_2O + CH_4$ complexes but will be present if $H_2O + CH_4$ complexes occur in the interlayer. When CH_4 is present, the reflection may be characteristic for the methane complex intercalation. The 22-Å spacing is a result of a structural unit involving methane hydrate (cell dimension of ~12 Å) and montmorillonite (d value of ~9.8 Å of the 2:1 silicate layer).

Results of the interaction experiments of natural marine I-S mixtures and hydrates showed clear and sharp peaks in the XRD pattern at 3.46, 3.32 and 3.20 Å corresponding to the methane hydrate nucleating in pore spaces, but there was no evidence of the characteristic 22-Å reflection found by Koster van Groos and Guggenheim (2009) where smectite reacts with methane to form complexes (Figure 5).

In the conducted experiments, and before exposure to methane, the observed *d*(001) was lower than 19 Å. To enhance the ability of clay swelling, one of the samples was exchanged with Na (designated here as Na-A2). However, the XRD showed that the *d*(001) was lower than 20 Å after saturation with water in the chamber, and consequently no methane hydrate was formed in the interlayer.

Although methane hydrate was present in the samples, the interlayer hydrate complex in the smectite component of I-S did not form under the conditions explored (Figure 6) and the samples used.

Computational Modeling

Previous experimental results proved that a smectite-methane hydrate complex can be formed for Na-exchanged montmorillonite and a Na-exchanged nontronite (Guggenheim and Koster van Groos, 2003; Koster van Groos and Guggenheim, 2009). This complex was considered for the modeling. Furthermore, in the above experiments, natural clay samples were used that are not pure swelling smectites. These samples have interstratified illite-smectite. The presence of a phyllosilicate with high tetrahedral charge, as illite, interlayered with smectite restricts swelling. The modeling of interstratified illite and smectite layers is beyond the scope of this work because models are too large and would require a high computational effort. Nevertheless, the effect of a significant tetrahedral charge in smectite

311 on a methane-hydrate complex model can be theoretically explored. Sato et al. (1996)
312 proved that the conversion of a beidellitic layer to an illitic layer preferably occurs during
313 early illitization. Before illitization, beidellite-like layers are formed from precursor
314 smectite. Therefore a Na-rich beidellite model was considered.
315
316 *Na-Montmorillonite and Na-Beidellite structures*
317 Geometry optimizations of Na-montmorillonite and Na-beidellite models were
318 performed at constant and variable volumes. The lattice parameters and the main
319 geometrical features are consistent with experimental values (Table 2). NPT ensemble MD
320 simulations were performed at ambient conditions (298.15 K and 1 atm) for 50 ps. The MD
321 simulations show that both models remain stable during the analysis. The mean basal *d*(001)
322 value for Na-montmorillonite is 12.08 Å, and 12.34 Å for Na-beidellite. This swelling is in
323 agreement with experiments (Posner and Quirk, 1964; Fu et al., 1990) and with previous
324 molecular simulations studies (Cygan et al., 2004). The Na..O distances (Table 2) indicate
325 the coordination of Na in the interlayer. These distances show that the Na ion is partly
326 coordinated with the O_{clay} species. In beidellite, this distance is shorter owing to the $^{IV}Al^{3+}$
327 which generates a high charge excess in the basal O atoms and thus the Coulombic
328 interactions with Na are stronger. In contrast, O_{water}-O_{water} values are close to experimental
329 neutron diffraction data for liquid water (Soper, 2000). Figure 7 shows the crystal structure
330 of Na-montmorillonite and Na-beidellite optimized at variable volume models.
331
332 *Crystal structure of methane hydrate*
333 Geometry optimization calculations for one unit cell of a methane hydrate model
334 (structure SI) were performed at constant and variable volume. The SPC model (Berendsen

et al., 1981), included in the CVFFH method, was used for water molecules. The lattice parameters and the main geometrical features are consistent with experimental values (Martos-Villa et al., 2013).

For the crystal structure models optimized at variable volume, XRD patterns were calculated and compared with experimental patterns (Fig. 8a). The patterns are similar and the crystal structure of methane hydrate can be successfully reproduced using these methods.

MD simulations of a 2 x 2 x 2 supercell with fully occupied methane hydrate were performed in the NPT ensemble with the CVFFH method at two different conditions: at pressure P = 40 bars and temperature T = 273 K under stable conditions (S-MH) (Fig. 8b); and at P = 1 bar and T = 726.85 K under unstable conditions (U-MH). All simulations were performed for 100 ps with a time step of 1 fs.

S-MH MD trajectories show that the methane hydrate model remains stable without significant distortions of the hydrogen bonding network. However, in U-MH, the hydrogen bonding network collapses and methane molecules tend to form aggregates with shorter C-C distances than in the crystal structure. The Radial Distribution Function (RDF) is a measure of the average distances (r) between pairs of atoms. The collapse of the methane hydrate structure can be observed on RDF peaks of C atoms in CH_4 molecules ($g_{C\text{-}C}$). Whereas the near C-C distance appears at 6.8 Å in S-MH, in U-MH this distance is between 3.4-4.6 Å. With rising temperature, methane hydrate will become less stable, and methane molecules tend to aggregate with shorter C-C distances than in the crystal lattice. This is consistent with previous computational studies (Bagherzadeh et al., 2012; Myshakin et al., 2009; Jiang et al., 2007).

Smectite-methane hydrate intercalates

359 Montmorillonite (Mnt-Hy) and beidellite (Bei-Hy) methane hydrate intercalates were
360 optimized at constant and variable volume. XRD patterns of the optimized models were
361 simulated (Fig. 9), obtaining a *d*(001) value close to 20 Å, in agreement with experimental
362 results obtained by Guggenheim and Koster van Groos (2003). Different configurations of
363 the methane hydrate complex along with the Na^+ hydrates in the interlayer were calculated.
364 The best hydrate geometry was obtained by removing the $Na(H_2O)_4$ in the interlayer, by
365 substituting ten methane molecules from the hydrate close to the tetrahedral sheet by Na^+
366 cations, and by distributing five Na^+ cations near each tetrahedral sheet. Geometry
367 optimization at variable volume of the intercalated structures produced lattice parameters
368 close to experimental values with an expanded c-axis value of 23.15Å in Mnt-Hy and
369 22.94Å in Bei-Hy intercalates (Table 2). The presence of an ordered methane-hydrate
370 complex in the interlayer of these smectites is demonstrated from RDF calculated distances.
371 The C-C distances in experimentally determined methane hydrate are observed at 6.80 Å,
372 whereas in Mnt-Hy and Bei-Hy these distances are 6.45 Å. Three O-O distance peaks are
373 found in experimentally determined methane hydrate at 2.8, 4.6 and 6.5 Å, and they occur at
374 2.75, 4.35 and 6.35 Å in Mnt-Hy and at 2.75, 4.45 and 6.45 Å in Bei-Hy intercalates.
375
376 MD simulations were performed within the NPT ensemble at different conditions for
377 Mnt-Hy and Bei-Hy intercalates: simulations involve stable conditions for methane hydrate
378 at P = 40 bars and T = 273 K (S-Mnt-Hy and S-Bei-Hy), and at unstable conditions at P = 40
379 bars and T = 320 K (U-Mnt-Hy and U-Bei-Hy). Simulations were performed for 100 ps by
380 stable MD and 50 ps for unstable MD with a time step of 1 fs. Figure 10 shows snapshots of
381 the initial and final configurations of the S-Mnt-Hy and S-Bei-Hy models of the MD
382 simulations. In both models, the intercalates are similar. In the final configurations at the end

383 of the MD simulations, the water molecules are slightly disordered although the methane
384 molecules remain in their initial positions.

385 Cell parameters were monitored during the simulations. Table 2 shows that the models
386 remained stable after each simulation with cell parameters and bond distances close to the
387 original Na-smectites. Each simulation showed a *d*(001) value close to the 20-Å
388 characteristic peak for smectite-methane-hydrate intercalates.

389 MD simulation results were analyzed by the RDF of C-C, C-O and O-O atom pairs taken
390 from 1000 configurations sampled each 100 fs of the simulations. The atom-pair peaks were
391 compared to previous results obtained by MD of the methane hydrate model under stable
392 conditions (S-MH). RDF profiles of O-O atom-pairs, $g_{O\text{-}O}$, display a common maximal peak
393 at $r_{O\text{-}O}$ = 2.8 Å, corresponding to the nearest distance between H_2O molecules linked by
394 hydrogen bonds (Fig. 11). The second and third maximal peaks appearing in the methane
395 hydrate model, at r_{OO} = 4.6 Å and 6.5 Å respectively, are well represented in the smectite-
396 hydrate models determined under stable conditions (S-Mnt-Hy and S-Bei-Hy). Those peaks
397 correspond to oxygen coordination in hydrates and only appear in O-O RDF profiles that
398 include the basal oxygen atoms. This result indicates that methane molecules close to the 2:1
399 layer surface are in sites formed by basal oxygen atoms and water molecules. These sites are
400 also observed in RDF profiles of C and O atoms $g_{C\text{-}O}$, where a maximal peak at $r_{C\text{-}O}$ = 4 Å
401 occurs for all MD simulations. This peak corresponds to water molecules surrounding the
402 methane. However, the remaining peaks at 6.6 Å, 8.0 Å, and 9.8 Å of the hydrate model
403 remain only in the stable MD simulation. These peaks are broader than in S-MH owing to
404 slight long-range disorder.

405 The RDF peaks of C atoms in CH_4 molecules, $g_{C\text{-}C}$, appear at $r_{C\text{-}C}$ ~7 Å and ~11 Å. These
406 peaks are intense in the stable smectite-hydrate complexes and coincident with S-MH peaks.

In the MD studied, there are small differences in the shape of these C-C peaks, as they are sharper in S-Mnt-Hy models. The sharper peaks indicate that the ordered structure of methane hydrate is better represented in montmorillonite than beidellite for the high-pressure and low-temperature conditions present. However, in unstable smectite-hydrate complexes, the most intense peak is observed at closer C-C distances than in the hydrate. This peak, at 3.9 Å, indicates methane-methane interactions consistent with methane clusters in bulk water (Bagherzadeh et al., 2012; Geng et al., 2009; Myshakin et al., 2009).

The mean square displacement (MSD) is a measure of the average distance a molecule travels during simulations. For a system at equilibrium, the particles will move in accordance with the equations of motion that define the system and, in general, will tend to diffuse away from their original location. For a stable crystal, the constituent atoms vibrate around their sites in the model without diffusing. Figure 12 illustrates MSD profiles of H_2O molecules in the smectite-methane-hydrate complex. In S-Mnt-Hy and S-Bei-Hy, MSD shows a solid profile with low diffusion, whereas in U-Mnt-Hy and U-Bei-Hy the increase in temperature gives more freedom to the model and facilitates the diffusion of H_2O molecules. There are differences between the montmorillonite and beidellite structures. In montmorillonite, MSD simulations show a lower diffusion of H_2O molecules than beidellite, indicating that montmorillonite-methane-hydrate intercalates are more stable than beidellite-methane-hydrate intercalates.

Based on MSD profiles, diffusion coefficients were calculated, yielding 0.027 $Å^2\ s^{-1}$ for S-Mnt-Hy; 0.038 $Å^2\ s^{-1}$ for S-Bei-Hy; 0.095 $Å^2\ s^{-1}$ for U-Mnt-Hy and 0.113 $Å^2\ s^{-1}$ for U-Bei-Hy.

Adsorption energies at constant volume

The adsorption energy of methane hydrate at the montmorillonite surface is -33.83 kcal mol^{-1} per unit cell, whereas in beidellite the adsorption energy is -23.31 kcal mol^{-1}. The adsorption energy calculated here refers to the process of immersion of methane hydrate into the smectite interlayer. This energy is more negative in the Mnt-Hy complex than in Bei-Hy, indicating that the Mnt-Hy complex is more stable. These energy differences relate to the location of the layer charge caused by tetrahedral vs octahedral site substitution in the clay mineral.

DISCUSSION

Modeling of hydrate complexes in smectite and comparison with experimental results

The present study focuses on the behavior of a methane hydrate complex in an expanded clay mineral structure, and the simulations support previous experimental data synthesizing methane hydrate-montmorillonite intercalates (Guggenheim and Koster van Groos, 2003; Koster van Groos and Guggenheim, 2009). MD simulations were performed using expanded Na-montmorillonite and Na-beidellite smectites with an initially ordered methane hydrate complex occupying the entire interlayer. The models used here simulate a larger smectite cell with a greater number of atoms than previous studies (Cygan et al., 2004), maintaining the periodic conditions for methane hydrate in the interlayer. These MD results demonstrate a stabilization of the methane hydrate intercalate in the expanded montmorillonite and beidellite structure corresponding to a *d*(001) value near 22 Å. These results agree with previous experimental (Guggenheim and Koster van Groos, 2003) and theoretical (Cygan et al., 2004) studies, but contrast with earlier theoretical calculations (Park and Sposito, 2003;

455 Titiloye and Skipper, 2000). In the latter, each methane molecule was solvated by 12-13
456 H_2O molecules and 8 oxygen atoms from the clay surface to complete a coordination shell in
457 an amorphous structure approaching a *d*(001) value close to 15 Å.

458 The comparison of XRD patterns presented in Figure 9 shows good agreement between
459 experimental patterns obtained *in situ* for a sample equilibrated at 267K and 41 atm methane
460 pressure for 126 h and a simulated diffraction pattern derived from theoretical structures
461 optimized at variable volume. Intense peaks at $d \sim 20$ Å and $d \sim 10$ Å are observed in both
462 simulated and experimental diffraction patterns, and these peaks represent the basal plane
463 reflections (001) and (002), respectively. These peaks are interpreted as methane-hydrate
464 complexes in either montmorillonite or beidellite.

465 RDF calculations show that water molecules from the methane hydrate are coordinated
466 with basal oxygen atoms from the smectite tetrahedral sheet, forming a smectite-methane
467 hydrate complex. Furthermore, the interlayer of this smectite-methane hydrate complex is
468 sufficiently periodic that the atomic coordinates of the methane-hydrate complex are similar
469 to those found in the methane-hydrate crystal structure.

470 Also, MSD calculations taken from MD simulations show differences in the behavior of
471 methane hydrate intercalates in montmorillonite vs beidellite models, where beidellite-
472 methane hydrate intercalates are less stable than montmorillonite-methane hydrate. Because
473 the difference between those two models is mainly the location of the layer charge in the
474 smectite (octahedral charge in montmorillonite, tetrahedral in beidellite), this is probably the
475 determining factor in the stability of smectite-methane-hydrate intercalates. This result is
476 also supported by the calculated adsorption energies, which are higher in the Mnt-Hy
477 complex than in Bei-Hy.

478 The simulations presented are in agreement with experimental data that shows a
479 significantly expanded interlayer (Guggenheim and Koster van Groos, 2003). Water
480 molecules form a hydrogen bonding network that encloses methane molecules in cages in
481 the interlayer. The water molecules close to the 2:1 layer form another cage enclosing
482 methane molecules with basal oxygen atoms.
483
484 *Experimental results*
485 Samples from a methane-bearing field show that no methane hydrate intercalate could be
486 formed under P(CH_4) and T conditions in the laboratory, although those conditions conform
487 to the stability conditions described by Guggenheim and Koster van Groos (2003) and
488 Koster van Groos and Guggenheim (2009). The failure of the smectite-methane hydrate
489 complex to crystallize may be related to various factors: for example, composition and layer
490 charge of the clay minerals and kinetics. As expected, the behavior of the clay samples, with
491 respect to the methane hydrate intercalation, differs from pure Na-exchanged smectite used
492 in previous studies (Guggenheim and Koster van Groos, 2003; Koster van Groos and
493 Guggenheim, 2009). An initial swelling with H_2O is crucial to form the methane hydrate
494 complex in the interlayer. The swelling capacities of smectites depend on physical-chemical
495 conditions such as salinity, interlayer cation composition, temperature and pressure.
496 Even after the clays were washed with distilled water to minimize salinity effects, the
497 lack of swelling persisted, as the samples have a significant proportion of divalent interlayer
498 cations. The expansion of smectites with the layer charge balanced by primarily divalent
499 ions, such as Mg^{2+}, Ca^{2+} is limited to d(001) values < 19 Å (Posner and Quirk, 1964).
500 Chemical composition data (Table 1 and Figure 4) show considerable amounts of divalent
501 ions like Mg^{2+} that clearly would restrict swelling. Furthermore, K^{+} has reduced swelling

behavior compared to Na^+. Thus, the formation of a smectite-methane-hydrate complex is affected by insufficient H_2O in the interlayer. To overcome this issue, a homoionic Na-exchanged clay sample was prepared to induce a significant increase in expansion capacity. Although expansion increased to *d*(001) values near 20 Å., no hydrate intercalate was obtained. However, additional factors may affect the formation of methane-hydrate complexes.

TEM images and XRD data show that discrete smectite is present as well as other clay minerals that may influence the intercalation of hydrates in the smectite interlayer. The samples also contain mica and kaolin plates, palygorskite fibers, and interstratified illite and smectite. The chemical analyses indicate that the smectite layers in the I-S interstratified layers have a tetrahedral charge higher than in montmorillonite and samples used in the previous work (Guggenheim and Koster van Groos, 2003; Koster van Groos and Guggenheim, 2009). This result suggests that the tetrahedral charge is an additional factor that limits the crystallization of methane hydrate complexes in the interlayer.

The theoretical calculations presented explore the local effect of the tetrahedral charge by comparing montmorillonite with beidellite. In both minerals, the adsorption of a methane hydrate complex in the interlayer is exothermic and thus favorable. However, this energy is more negative (more exothermic) in montmorillonite than in beidellite. In addition, the MD simulations show that the model for the methane hydrate complex is more periodic and stable in montmorillonite than in beidellite. The tetrahedral charge is located mainly at the basal oxygen atoms nearest the tetrahedral sites that are substituted by Al and which interact strongly with the H atoms of the water molecules closest to the tetrahedral sheets. The hydrogen bond network of the hydrate interacts with the remainder of the interlayer system to produce instability in the hydrate complex because there is a lower diffusion of the water

526 molecules in beidellite than in the montmorillonite system. However, the calculations show
527 that the energy difference between montmorillonite and beidellite with respect to the
528 methane- hydrate intercalate (where the greater the tetrahedral charge does not enhance the
529 formation of the hydrate complex) is relatively favorable.

530 The time scale, and therefore kinetics, of the reactions may also be an important control
531 in the nucleation of a methane hydrate complex in the interlayer of smectites. In mud-
532 volcano areas, and after extrusion of the mud to the ocean floor, the sediments are in contact
533 with sea-water and can mix with fluids and methane expelled by the mud extrusion. The
534 pore water composition described in other mud volcanoes of the area (Scholzt et al., 2009;
535 Hensen et al., 2007) are, on average, depleted below sea-water values in Cl, Na, Mg and K,
536 and Ca unless they originate from a deeper brine source. This low salinity is believed to be
537 caused by the mixing of seawater with fluids from water released by the dehydration and
538 illitization reactions involving smectite at depth which would promote swelling of smectite
539 in the sediment closer to the seafloor. Therefore, an increase in the swelling capacities of
540 smectite layers is expected in mud-volcano areas where the clay mineralogy originates from
541 deeper areas and where smectite-illite diagenetic changes have occurred at depth (Scholzt et
542 al., 2009, Hensen et al., 2007, Mata et al., 2012).

543 The nature of the experiments may also affect the kinetics of the reactions. Clays are
544 excellent sealants, and the ability of methane to diffuse through a clay surface may be
545 limited in an experiment that is maintained over a few weeks. As noted previously by Koster
546 van Groos and Guggenheim (2009), the formation of ice prior to the formation of a methane
547 hydrate complex may seal the edges of the clay hydrate particle, thereby further preventing
548 methane diffusion into the interlayer. For these reasons, conclusions should be considered
549 tentative.

The detailed characterization of the clays, as well as preliminary B isotopic analysis (Mata et al., 2012), have shown that mixed-layer illite-smectite phases and other clay minerals are present in the mud volcano samples, implying diagenetic changes at depth that gave rise to a progressive illitization of smectite. Mud volcanoes in the marine environment usually involve a mix of diagenetic and detrital clays in a rich fluid environment. Physical (fluid transport) mixing of different types of particles will give rise to a wide dispersion of clay minerals of differing chemical composition. This fluid transport may allow smectite to coexist with interstratified mixtures of illite with ordering sequences from R0 to R1 to illite in a fluid-rich environment. Samples from shallow sources will have a greater smectite content and thus methane hydrate complexes in the smectite may became more prevalent in nature. Hence, the existence of smectite-methane hydrate complexes in nature is limited to clays that can intercalate a hydrate sufficiently. Thus, expansion characteristics of the clay are important, in addition to the source of layer charge, reaction rates at these low temperatures, and the presence of divalent exchangeable cations.

IMPLICATIONS

One of the important consequences of these interactions is the possibility of the methane being incorporated or sequestered in clays. Koster van Groos and Guggenheim, (2009) conclude that if 10% of ocean-floor smectite is in a physical/chemical environment that allows it to swell and, therefore, intercalate with methane hydrate, a maximum of 1.5×10^5 Gt C could be sequestered in smectites, assuming a 5% methane content of the smectite complex. Those calculations were based on previous estimates of ocean smectite distributions (Poldervaart, 1955; Windom, 1976; Hay et al., 1988) and methane content

574 present in gas hydrates (Kvenvolden 1999; MacDonald 1990; Buffett and Archer 2004)
575 ranging from 500-7000 Gt C. However, the global abundance of gas hydrates in marine
576 sediments is poorly constrained. Geochemical transport-reaction modeling (Archer et al.,
577 2009, Burwicz et al., 2011) and the application of transfer functions (Wallman et al., 2012,
578 Piñero et al., 2013) suggest average values of 550 Gt of C stored in gas hydrates. Although
579 the methane stored as smectite-hydrate complexes is considerably less than that initially
580 estimated by Koster van Groos and Guggenheim (2009), the amount of smectite in the
581 seabed is extremely high, thus the amount of methane stored as smectite-hydrate complexes
582 is significant. In addition, large occurrences of thermogenic methane hydrate have been
583 found in permafrost-affected sedimentary rocks (Stotler et al., 2010). These deposits also
584 contain clay and surfactant substances, possibly producing smectite-methane hydrate
585 complexes.

586 This study contributes to a better chemical characterization of natural smectites from a
587 methane-field area, with input of molecular models and previous experimental data. More
588 common compositions and the limitations of some clays to form methane-hydrate
589 complexes on the seafloor are considered. Smectite is a pervasive clay mineral on the ocean
590 floor and it is present at continental margins to oceanic ridges (Chamley, 1997; Griffin et al.,
591 1968). Clay distributions, paleoclimatic interpretations and processes related to
592 hydrothermal activity have been considered recently as a major issue of study (Clauer et al.,
593 1990; Alt, 2000; Cole and Shaw, 1983; Singer, 1984; Thiry, 2000) and there are recent
594 studies of marine methane-bearing sediments, described as clay- and smectite-rich (Dearman
595 et al., 2009; Ertefai et al., 2010; Ji et al., 2012). Nevertheless, such studies are incomplete if
596 they do not consider detailed structural and compositional data of the clays, including the

type of interlayer cations of marine smectites. These data are required to predict smectite-methane behavior in rich-gas environments.

605

606 **ACKNOWLEDGMENTS**

607 Funding for this work came from RNM-3581 CADHYS project and a doctoral
608 scholarship of the Junta de Andalucía (Spain). Samples were obtained in the framework of
609 MOUNDFORCE - EUROCORE-EUROMARGINS 01-LEC-EMA06F and TASYO (MAR-
610 98-0209) projects, on board of RVs Hespérides and Cornide de Saavedra respectively. The
611 authors thank H. Heinz for his useful discussions and for facilitating the use of force fields,
612 W. Kuhs for the availability of crystal atomic data of methane hydrate, M. Mar Abad of the
613 Centro de Instrumentación Científica (CIC) of Granada, and PAIDI-groups RNM-328 and
614 RNM-363 of the Andalusia Government for the financial support, the Supercomputational
615 Center of the Granada University (UGRGRID), and the Centro Técnico de Informática of
616 CSIC.

617

References

Abid, I.A., Hesse, R., Harper, J.D. (2004) Variations in mixed-layer illite/smectite diagenesis in the rift and post-rift sediments of the Jeanne d'Arc Basin, Grand Banks offshore Newfoundland, Canada. Canadian Journal of Earth Sciences, 41, 401-429.

Accelrys Software, Inc. (2009) Materials Studio, version 5.0. San Diego, CA.

Alt, J.C. (2000) Very low grade hydrothermal metamorphism of basic igneous rocks. In: Very Low Grade Metamorphism. M. Frey and D. Robinson, eds., Blackwell Scientific, 169-201.

Andersen, H.C. (1980) Molecular dynamics simulations at constant pressure and/or temperature. Journal of Chemical Physics, 72, 9173-9183.

Anderson, B.J., Tester, J.W., Borghi, G.P., Trout, B.L. (2005) Properties of inhibitors of methane hydrate formation via molecular dynamics simulations. Journal of the American Chemical Society, 125, 17852-17862.

Archer, D. (2007) Methane hydrate stability and anthropogenic climate change. Biogeosciences, 4, 993–1057.

Archer, D., Buffet, B., and Brovkin, V. (2009) Ocean methane hydrates as a slow tipping point in the global carbon cycle. Proceedings of the National Academy of Sciences of the United States of America, 106, 20596–20601.

Aringhieri, R. (2004) Nanoporosity characteristics of some natural clay minerals and soils. Clays and Clay Minerals, 52, 700-704.

Aróstegui, J., Sangüesa, F.J., Nieto, F., Uriarte, J.A. (2006) Thermal models and clay diagenesis in the Tertiary-Cretaceous sediments of the Alava block (Basque-Cantabrian basin, Spain). Clay Minerals, 41, 791-809.

Bagherzadeh, S.A., Englezos, P., Alavi, S., Ripmeester, J.A. (2012) Molecular simulation of non-equilibrium methane hydrate decomposition process. The Journal of Chemical Thermodynamics, 44, 13-19.

Berendsen, H.J.C., Postma, J.P.M., van Gusteren, W.F., Hermans, J. (1981) Interaction models for water in relation to protein hydration, in: Intermolecular Forces, edited by B. Pullman, pp. 331–342, D. Reidel Publishing Company, Dordrecht.

Berendsen, H.J.C., Postma, J.P.M., van Gusteren, W.F., DiNola, A., Haak, J.R. (1984) Molecular dynamics with coupling to an external bath. Journal of Chemical Physics, 37, 185-192.

Besler, B.H., Merz Jr., K.M., Kollman, P.A. (1990) Atomic charges derived from semiempirical methods. Journal of Computational Chemistry, 11, 431-439.

665 Buffet, B.A. (2000) Clathrate hydrates. Annual Review of Earth and Planetary Science
666 Letters, 28, 477-507.
667
668 Buffett, B.A. and Archer, D.E. (2004) Global inventory of methane clathrate: Sensitivity to
669 changes in environmental conditions. Earth Planetary Science Letters, 227, 185–199.
670
671 Burwicz, E., Rupke, L. H., Wallmann, K. (2011) Estimation of the global amount of
672 submarine gas hydrates formed via microbial methane formation based on numerical
673 reaction transport modeling and a novel parameterization of Holocene sedimentation.
674 Geochimica et Cosmochimica Acta, 75, 4562–4576.
675
676 Cha, S.B., Ouar, H., Wildeman, T.R., Sloan, E.D. (1988) A third-surface effect on hydrate
677 formation. Journal of Physical Chemistry, 92, 6492-6494.
678
679 Chamley, H. (1997) Clay mineral sedimentation in the ocean. In: Paquet, H., Clauer, N.
680 (Eds.), Soils and Sediments. Mineralogy and Geochemistry. Springer, Berlin, 269–302.
681
682 Chassefiére, E. (2009) Metastable methane clathrate particles as a source of methane to the
683 martian atmosphere. Icarus, 204, 137-144.
684
685 Chastain, B.K. and Chevrier, V. (2007) Methane clathrate hydrates as a potential source for
686 martian atmospheric methane. Planetary and Space Science, 55, 10, 1246-1256.
687

688 Chihaia, V., Adams, S., Kuhs, W.F. (2005) Molecular dynamics simulations of properties of
689 a (001) methane clathrate hydrate surface. Chemical Physics, 317, 208-225.
690
691 Chung, F.H. (1974, a) Quantitative interpretation of X-ray diffraction patterns. I. Matrix
692 flushing method of quantitative multicomponent analysis. Journal of Applied
693 Crystallography, 7, 519-525.
694
695 Chung, F. H. (1974, b) Quantitative interpretation of X-ray diffraction patterns of mixtures.
696 II. Adiabatic principle of X-ray diffraction analysis of mixtures. Journal of Applied
697 Crystallography, 7, 526-531.
698
699 Chung, F.H. (1975) Quantitative interpretation of X-ray diffraction patterns of mixtures. III.
700 Simultaneous determination of a set of reference intensities. Journal of Applied
701 Crystallography, 8, 17-19.
702
703 Clauer, N., O'Neil, J.R., Bonnot-Courtois, C., Holtzappfel, T. (1990) Morphological,
704 chemical and isotopic evidence for an early diagenetic evolution of detrital smectite in
705 marine sediments. Clays and Clay Minerals, 38, 33–46.
706
707 Clennell, M.B., Hovland, M., Booth, J.S., Henry, P., Winters, W.J. (1999) Formation of
708 natural gas hydrates in marine sediments 1. Conceptual model of gas hydrate growth
709 conditioned by host sediment properties. Journal of Geophysical Research, 104, 22985-
710 23003.

711 Cole, T.G. and Shaw, S-H. (1983) The nature and origin of authigenic smectites in some
712 recent marine sediments. Clay Minerals, 18, 239–252.
713
714 Conde, M.V., Vega, C., McBride, C., Noya, E.G., Ramirez, R., Sesé, L.M. (2010) Can gas
715 hydrate structures be described using classical simulations?. Journal of Physical Chemistry,
716 132, 114503.
717
718 Cygan, R.T., Guggenheim, S., Koster van Groos, A.F. (2004) Molecular models for the
719 intercalation of methane hydrate complexes in montmorillonite clay. Journal of Physical
720 Chemistry B, 108, 15141-15149.
721
722 Davie, M.K., Zatsepina, O.Y., Buffett, B.A. (2004) Methane solubility in marine hydrate
723 environments. Marine Geology, 203, 177-184.
724
725 Dearman, J.L., Wilson, W.W., Rogers, R.E., Zhang, G. (2009) Gas-hydrate promotion by
726 smectite–bioproduct interactions. Marine Chemistry, 115, 21-30.
727
728 Du, Q., Li, P., Liu, P., Huang, R. (2008) Molecular potential energies in dodecahedron cell
729 of methane hydrate and dispersion correction for DFT. Journal of Molecular Graphics and
730 Modeling, 27, 140-146.
731
732 Ehlmann, B.L., Mustard, J.F., Fassett, C.I., Schon, S.C., Head, J.W., DesMarais, D.J., Grant,
733 J.A., Murchie, S.L. (2008) Clay minerals in delta deposits and organic preservation potential
734 on Mars. Nature Geoscience, 1, 355–358.

Ertefai, T.F., Heuer, V.B., Prieto-Mollar, J., Vogt, C., Sylva, S.P., Seewald, J., Hinrichs, K. (2010) The biogeochemistry of sorbed methane in marine sediments. Geochimica et Cosmochimica Acta, 74, 6033-6048.

Ferrage, E., Vidal, O., Mosser-Ruck, R., Cathelineau, M., Cuadros, J. (2011) Reinvestigation of smectite illitization in experimental hydrothermal conditions: Results from X-ray diffraction and transmission electron microscopy. American Mineralogist, 96, 207-223.

Frisch, M.J., Trucks, G.W., Schlegel, H.B., Scuseria, G.E., Robb, M.A., Chesseman, J.R., Zarzewki, V.G., Montgomery, J.A., Stratmann, R.E., Burant, J.C., Dapprich, S., Millam, J.M., Daniels, A.D., Kudin, K.N., Strain, M.C., Farkas, O., Tomasi, J., Barone, V., Cossi, M., Cammi, R., Mennucci, B., Pomelli, C., Adamo, C., Clifford, S., Ochterski, J., Petersson, G.A., Ayala, P.Y., Cui, Q., Morokuma, K., Malick, D.K., Rabuck, A.D., Raghavachari, K., Foresman, J.B., Cioslowski, J., Ortiz, J.V., Stefanov, B.B., Liu, G., Liashenko, A., Piskorz, P., Komaromi, I., Gomperts, R., Martin, R.L., Fox, D.J., Keith, T.A., Al-Laham, M.A., Peng, C.Y., Nanayakkara, A., Gonzalez, C., Challacombe, M., Gill, P.M.W., Johnson, B.G., Chen, W., Wong, M.W., Andres, J.L., Head-Gordon, M., Replogle, E.S., Pople, J.A. (2004) Gaussian 03 (RevisionA.1), Gaussian, Inc., Pittsburgh, PA.

Fu, M.H., Zhang, Z.Z., Low, P.F. (1999) Changes in the properties of a montmorillonite-water system during the adsorption and desorption of water: hysteresis. Clays and Clay Minerals, 38, 485-492.

Geng, C., Wen, H., Zhou, H. (2009) Molecular simulation of the potential of methane reoccupation during the replacement of methane hydrate by CO_2. Journal of Physical Chemistry, 113, 5463-5469.

Gough, R.V., Tolbert, M.A., McKay, C.P., Toon, O.B. (2010) Methane adsorption on a martian soil analog: An abiogenic explanation for methane variability in the martian atmosphere. Icarus, 207, 165-174.

Gournis, D., Lappas, A., Karakassides, M.A., Többens, D., Moukarika, A. (2008) A neutron diffraction study of alkali cation migration in montmorillonites. Physics and Chemistry of Minerals, 35, 49-58.

Griffin, J.J., Windom, H., Goldberg, E.D. (1968) The distribution of clay minerals in the world oceans. Deep-Sea Research, 15, 433–445.

Guggenheim, S. and Koster van Groos, A.F. (2003) New gas-hydrate phase: Synthesis and stability of clay-methane hydrate intercalate. Geology, 31, 653-656.

Hay, W.W., Sloan II, J.L., Wold, C.N. (1988) Mass/age distribution of sediments on the ocean floor and the global rate of sediment subduction. Journal of Geophysical Research, 93, 14933–14940.

Heinz, H., Koerner, H., Anderson, K.L., Vaia, R.A., Farmer, B.L. (2005) Force field for mica-type silicates and dynamics of octadecylammonium chains grafted to montmorillonite. Chemistry of Materials, 17, 5658-5669.

Henry, P., Thomas, M., Clennell, M.B. (1999) Formation of natural gas hydrates in marine sediments 2. Thermodynamic calculations of stability conditions in porous sediments. Journal of Geophysical Research, 104, 23005-23022.

Hensen, C., Nuzzo, M., Hornibrook, E., Pinheiro, L.M., Bock, B., Magalhaes, V.H., Bruckmann, W. (2007) Sources of mud volcano fluids in the Gulf of Cadiz-indications for hydrothermal imprint. Geochimica et Cosmochimica Acta, 71, 1232–1248.

Hernández-Laguna, A., Escamilla-Roa, E., Timón, V., Dove, M.T., Sainz-Díaz, C.I. (2006) DFT study of the cation arrangements in the octahedral and tetrahedral sheets of dioctahedral 2:1 phyllosilicates. Physics and Chemistry of Minerals, 33, 655-666.

Hinrichs K. U., Hayes J. M., Bach W., Spivack A. J., Hmelo L. R., Holm N. G., Johnson C. G., Sylva S. P. (2006) Biological formation of ethane and propane in the deep marine subsurface. Proceedings of the National Academy of Sciences, USA, 103, 14684–14689.

Hower J., Eslinger E.V., Hower M.E., Perry E.A. (1976) Mechanism of burial metamorphism of argillaceous sediments: 1. Mineralogical and chemical evidence. Geological Society of America Bulletin, 87, 725 - 737.

806 Jager, M.D. and Sloan, E.D. (2001) The effect of pressure on methane hydration in pure
807 water and sodium chloride solutions. Fluid Phase Equilibria, 185, 89-99.
808
809 Ji, L., Zhang, T., Milliken, K.L., Qu, J., Zhang, X. (2012) Experimental investigation of
810 main controls to methane adsorption in clay-rich rocks. Applied Geochemistry, 27, 2533-
811 2545.
812
813 Jiang, H., Jordan, K.D., Taylor, C.E. (2007) Molecular dynamics simulations of methane
814 hydrate using polarizable force fields. Journal of Physical Chemistry B, 111, 6486-6492.
815
816 Kerr, P.F., Drew, J.M., Richardson, D.S. (1970) Mud volcanoes clays, Trinidad, West
817 Indies. American Association of Petroleum Geologists Bulletin, 54, 2101–2110.
818
819 Klapproth A. (2002) Strukturuntersuchungen an Methan- und Kohlenstoffdioxid-Clathrat-
820 Hydraten, Ph.D. Thesis, Georg-August-Universitat, Gottingen, Germany.
821
822 Klauda, J.B. and Sandler, S.I. (2002) Ab initio intermolecular potentials for gas hydrates and
823 their predictions. Journal of Physical Chemistry B, 106, 5722-5732.
824
825 Kopf, A.J. (2002) Significance of mud volcanism. Reviews of Geophysics, 40, 2-52.
826
827 Koster van Groos, A.F., Guggenheim, S., Cornell, C. (2003) Environmental chamber for
828 powder X-ray diffraction for use at elevated pressures and low temperatures: Review of
829 Scientific Instruments, 74, 273–275.

Koster van Groos, A.F. and Guggenheim, S. (2009) The stability of methane hydrate intercalates of montmorillonite and nontronite: Implications for carbon storage in ocean-floor environments. American Mineralogist, 94, 372-379.

Kvenvolden, K.A. (1998) A primer on the geological occurrence of gas hydrate. Geological Society, London, Special Publications, 137, 9-30.

Kvenvolden, K.A. (1999) Potential effects of gas hydrate on human welfare. Proceedings of the National Academy of Sciences, 96, 3420–3426.

Lee, J. and Guggenheim, S. (1981) Single crystal X-ray refinement of pyrophyllite-1Tc. American Mineralogist, 66, 350-357.

León, R., Somoza, L., Medialdea, T., Vázquez, J.T., González, F.J., López-González, N., Casas, D., Mata, M.P., Fenández-Puga, M.C., Jiménez-Moreno, C.J., Díaz-del-Río, V. (2012) New discoveries of mud volcanoes on the Moroccan Atlantic continental margin (Gulf of Cádiz): morpho-structural characterization. Geo-Marine Letters, 32, 473-488.

Liang, S. and Kusalik, P.G. (2010) Explorations of gas hydrate crystal growth by molecular simulations. Chemical Physics Letters, 494, 123-133.

MacDonald, G.J. (1990) The future of methane as an energy resource. Annual Review of Energy, 15, 53–83.

Machida, S., Hirai, H., Kawamura, T., Yamamoto, Y., Yagi, T. (2006) A new high-pressure structure of methane hydrate surviving to 86 GPa and its implications for the interiors of giant icy planets. Physics of Earth and Planetary Interiors, 155, 170-176.

Martín-Puertas, C., Mata, M.P., Fernández-Puga, M.C., Díaz-del-Río, V., Vázquez, J.T., Somoza, L. (2007) A comparative mineralogical study of gas-related sediments of the Gulf of Cádiz. Geo-Marine Letters, 27, 223-235.

Martos-Villa, R., Francisco-Márquez, M., Mata, P., Sainz-Díaz, C.I. (2013) Crystal structure, stability and spectroscopic properties of methane and CO_2 hydrate. Journal of Molecular Graphics and Modelling, 44, 253-265.

Mata. M.P., Williams, L.B., Nieto., F., Martos, R., Sainz-Díaz, C.I. (2012) Preliminary B and Li isotope data of illite/smectite from mud volcano sediments from de Gulf of Cádiz. Macla, 16, 100-101.

Milkov, A. V. (2000) Worldwide distribution of submarine mud volcanoes and associated gas hydrates. Marine Geology, 167, 29–42.

Milkov, A.V. (2005) Molecular and stable isotope compositions of natural gas hydrates: A revised global dataset and basic interpretations in the context of geological settings. Organic Geochemistry, 36, 681–702.

878 Molina-Montes, M.E., Donadio, D., Sainz-Díaz, C.I., Hernández-Laguna, A., Parrinello, M.
879 (2008) DFT research on the dehydroxylation reaction of pyrophyllite 1. First-principle
880 molecular dynamics simulations. Journal of Physical Chemistry B, 112, 7051-7060.
881
882 Myshakin, E. M., Jiang, H., Warzinski, R. P., Jordan, K.D. (2009) Molecular dynamics
883 simulations of methane hydrate decomposition. Journal of Physical Chemistry A, 113, 1913-
884 1921.
885
886 Park, S.-H. and Sposito, G. J. (2003) Do montmorillonite surfaces promote methane hydrate
887 formation? monte carlo and molecular dynamics simulations. Journal of Physical Chemistry
888 B, 107, 2281-2290.
889
890 Piñero, E., Marquardt, M., Hensen, C., Haeckel, M., Wallmann, K. (2013) Estimation of the
891 global inventory of methane hydrates in marine sediments using transfer functions.
892 Biogeosciences, 10, 959-975.
893
894 Poldervaart, A. (1955) Chemistry of the Earth's crust. In A. Poldervaart, Ed., Crust of the
895 Earth. Special Paper Geological Society of America, 62, 119–144.
896
897 Posner, A. M. and Quirk, J. P. (1964) Changes in basal spacing of montmorillonite in
898 electrolyte solutions. Journal of Colloid Science, 19, 798-812.
899
900 Robertson, A.H.F. and Kopf, A. (1998) Tectonic setting and processes of mud volcanism on
901 the Mediterranean Ridge accretionary complex: evidence from Leg 160. In: Robertson,

902 A.H.F, Emeis, K.C., Richter, C. et al (eds) Proc ODP Sci Results 160. Ocean Drilling
903 Program, College Station, TX, 665–680.
904
905 Rodger, M. (1990) Stability of Gas Hydrates. Journal of Physical Chemistry, 94, 6080-6089.
906
907 Sainz-Díaz, C.I., Palin, E.J., Hernández-Laguna, A., and Dove, M.T. (2003) Octahedral
908 cation ordering of illite and smectite. Theoretical exchange potential determination and
909 Monte Carlo simulations. Physics and Chemistry of Minerals, 30, 382-392.
910
911 Sainz-Díaz. C.I., Francisco-Márquez, M., Vivier-Bunge, A. (2011) Adsorption of
912 polyaromatic heterocycles on pyrophyllite surface by means of different theoretical
913 approaches. Environmental Chemistry, 8, 429-440.
914
915 Sato, T., Murakami, T., Watanabe, T. (1996) Change in layer charge of smectites and
916 smectite layers in illite/smectite during diagenetic alteration. Clays and Clay Minerals, 44,
917 460-469.
918
919 Scholz, F., Hensen, C., Reitz, A., Romer, R.L., Liebetrau, V., Meixner, A., Weise, S.M.,
920 Haeckel, M. (2009) Isotopic evidence ($^{87}Sr/^{86}Sr$, $\delta^{7}Li$) for alteration of the oceanic crust at
921 deep-rooted mud volcanoes in the Gulf of Cadiz, NE Atlantic Ocean. Geochimica et
922 Cosmochimica Acta, 73, 18, 5444-5459.
923
924 Singer, A. (1984) The paleoclimatic interpretation of clay minerals in sediments - A review.
925 Earth Science Reviews, 21, 251–293.

926

927 Sloan, E.D. (1998) Physical/chemical properties of gas hydrates and application to world
928 margin stability and climatic change. Geological Society, London, Special publications, 137,
929 31-50.

930

931 Somoza, L., Díaz-del-Río, V., León, R., Ivanov, M., Fernández-Puga, M.C., Gardner, J.M.,
932 Hernández-Molina, F.J., Pinheiro, L.M., Rodero, J., Lobato, A., Maestro, A., Vazquez, J.T.,
933 Medialdea, T., Fernández-Salas, L.M. (2003). Seabed morphology and hydrocarbon seepage
934 in the Gulf of Cádiz mud volcano area: Acoustic imagery, multibeam and ultra-high
935 resolution seismic data. Marine Geology, 195, 153-176.

936

937 Soper, A.K. (2000) The radial distribution functions of water and ice from 220 to 673 K and
938 at pressures up to 400 Mpa. Chemical Physics, 258, 121-137.

939

940 Stotler, R.L, Frape, S.K., Ahonen, L., Clark, I., Greene, S., Hobbs, M., Johnson, E.,
941 Lemieux, J.M., Peltier, R., Pratt, L., Ruskeeniemi, T., Sudicky, E., Tarasov, L. (2010) Origin
942 and stability of a permafrost methane hydrate occurrence in the Canadian Shield. Earth and
943 Planetary Science Letters, 296, 384-394.

944

945 Sun, R. and Duan, Z. (2007) An accurate model to predict the thermodynamic stability of
946 methane hydrate and methane solubility in marine environments. Chemical Geology, 244,
947 248-262.

948

949 Thiry, M. (2000) Palaeoclimatic interpretation of clay minerals in marine deposits: an
950 outlook from the continental origin. Earth-Science Reviews, 49, 201–221.
951
952 Titiloye, J.O, and Skipper, N.T. (2000) Computer simulation of the structure and dynamics
953 of methane in hydrated Na-smectite clay. Chemical Physics Letters, 329, 23-28.
954
955 Titiloye, J.O. and Skipper, N.T. (2001) Molecular dynamics simulation of methane in
956 sodium montmorillonite clay hydrates at elevated pressures and temperatures. Molecular
957 Physics, 99, 899-906.
958
959 Velde, B. and Vasseur, G. (1992) Estimation of the diagenetic smectite to illite
960 transformation in time-temperature space. American Mineralogist, 77, 967-976.
961
962 Wallmann, K., Piñero, E., Burwicz, E., Haeckel, M., Hensen, C., Dale, A., and Ruepke, L.
963 (2012) The global inventory of methane hydrate in marine sediments: a theoretical approach,
964 Energies, 5, 2449–2498.
965
966 Wang, C.C., Juang, L.C., Hsu, T.C., Lee, C.K., Lee, J.F., Huang, F.C. (2004) Adsorption of
967 basic dyes onto montmorillonite. Journal of Colloid and Interface Science, 273, 80-86.
968
969 Windom, H.L. (1976) Lithogeneous material in marine sediments. In J.P. Riley and R.
970 Chester, Eds., Chemical Oceanography, p. 103–135. Academic Press, London.
971

Wray, J.J. and Ehlmann, B.L. (2011) Geology of possible Martian methane source regions. Planetary and Space Science, 59, 196-202.

Zhang, J. and Pan, Z. (2011) Effect of potential energy on the formation of methane hydrate. Journal of Petroleum Science and Engineering, 76, 148-154.

Zhang, J., Dong, H., Liu, D., Fischer, T.B., Wang, S., Huang, L. (2012) Microbial reduction of Fe(III) in illite–smectite minerals by methanogen Methanosarcina mazei. Chemical Geology 292, 23, 35-44.

Zhou, Q., Lu, X., Liu, X., Zhang, L., He, H., Zhu, J., Yuan, P. (2011) Hydration of methane intercalated in Na-smectites with distinct layer charge: Insights from molecular simulations. Journal of Colloid and Interface Science, 355, 237-242.

Zitter, T.A.C. (2004) Mud volcanism and fluid emissions in Eastern Mediterranean neotectonic zones. PhD thesis, Vrije Universiteit, Amsterdam.

Captions of Figures

Figure 1.- Cation distributions in the initial models of montmorillonite (a) and beidellite (b). From left to right: Full view, upper tetrahedral 2:1 sheet, lower tetrahedral 2:1 sheet, and octahedral sheet. Light-gray polyhedra represent tetrahedral Si, dark-gray octahedral and tetrahedral Al, black octahedral Mg substitutions and light-gray balls interlayer Na cations.

Figure 2.- Tetrahedrally (a) and octahedrally (b) coordinated Na hydrates. H, O, and Na atoms are represented in white, black and dark-gray balls respectively.

Figure 3.- TEM micrographs of the major phases present. a) Interstratified illite-smectite particles on M3 sample; b) Interstratified illite-smectite and palygorstite fibers in the M8 sample; c) Smectite flakes in the M4 sample; d) Smectite aggregates, illite-smectite interstratifications and kaolinite particles in the A2 sample. Sme: Smectite; Kln: Kaolinite; Plg: Palygorskite; I/S: Illite-smectite interstratified.

Figure 4.- Interlayer K as a function of tetrahedral Al obtained from chemical microanalysis. Sme: Smectite; I/S: Illite-smectite interstratified; Ilt: Illite.

Figure 5.- Powder XRD patterns of the clay samples at $P(CH_4)$=58 bar in the sample chamber. MH: Methane-hydrate peaks.

Figure 6.- Powder XRD patterns of the clay M12 sample during the swelling process with water. a) Starting material at room temperature; b) with additional water after 1 hour at 12 ºC; c) at 12 ºC after 2.5 hours; d) at 12ºC after 3 hours; e) at 4ºC after 3.5 hours of the beginning of swelling process; f) after 4 hours at 4ºC, completely swollen.

Figure 7.- Crystal structure of the Na-montmorillonite (a) and Na-Beidellite (b) models optimized at variable volumes. Light-gray polygons represent tetrahedral Si, dark-gray polygons octahedral and tetrahedral Al, black polygons octahedral Mg substitutions, and light-gray balls represent interlayer Na cations. H and O atoms from water molecules are represented in light-gray and black sticks respectively.

Figure 8-. Methane hydrate crystal structure. XRD pattern of optimized and experimental (Klapproth, 2002) structures (a); and snapshot of 2 x 2 x 2 supercell structure from Molecular Dynamics simulation at 273 K and 40 bar after 100 ps (b). Methane atoms are highlighted as spheres. The O, H, and C atoms are in black, white, and dark-gray colors respectively.

Figure 9. Comparison of the experimental XRD pattern (Guggenheim and Koster van Groos, 2003) and simulated XRD patterns for the montmorillonite-methane hydrate complex (Mnt-Hy, left) and beidellite-methane hydrate intercalates (Bei-Hy, right).

Figure 10.- Snapshots of initial and final configurations of smectite-methane hydrate intercalates (Mnt-Hy, left and Bei-Hy, right) in the MD trajectories. The methane and sodium atoms are highlighted as spheres. Yellow polygons are tetrahedral Si, pink polygons are octahedral and tetrahedral Al, dark-green polygons represent octahedral Mg substitutions and blue balls represent interlayer Na cations. H and O atoms from water molecules are represented in light-gray and red sticks respectively. C atoms from methane molecules are light-green balls.

Figure 11.- RDFs of C-C (a), C-O (b), and O-O (c), atoms of smectite-methane hydrate intercalates obtained from MD simulations and compared with methane hydrate crystal structure (SMH).

Figure 12.- MSD of water molecules in smectite-methane hydrate intercalates obtained from MD simulations.

a

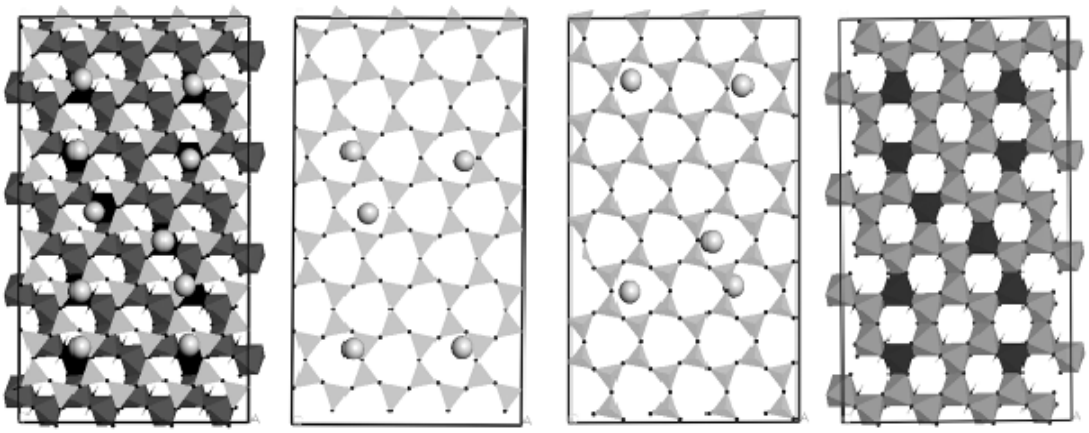

b

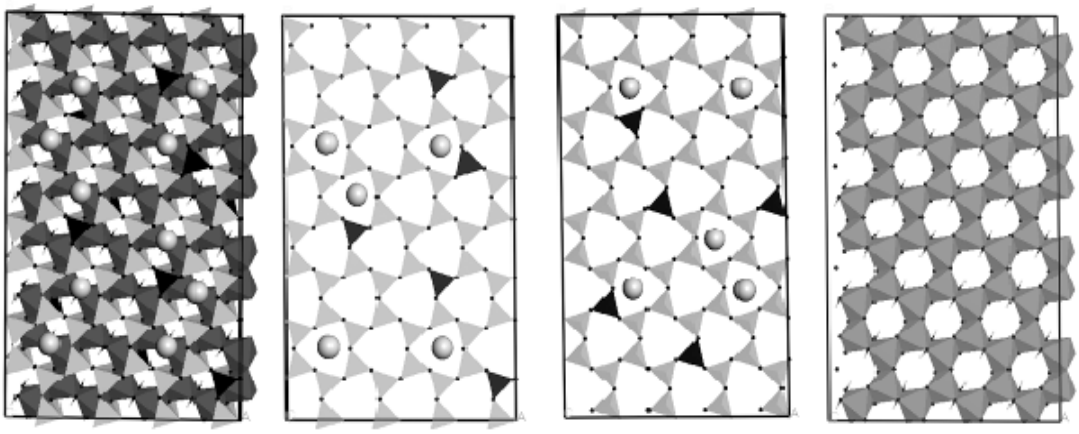

Fig. 1.-

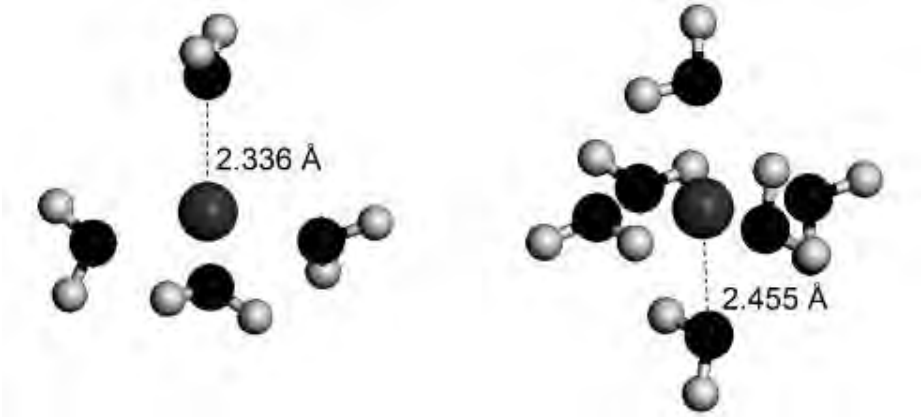

Fig. 2.-

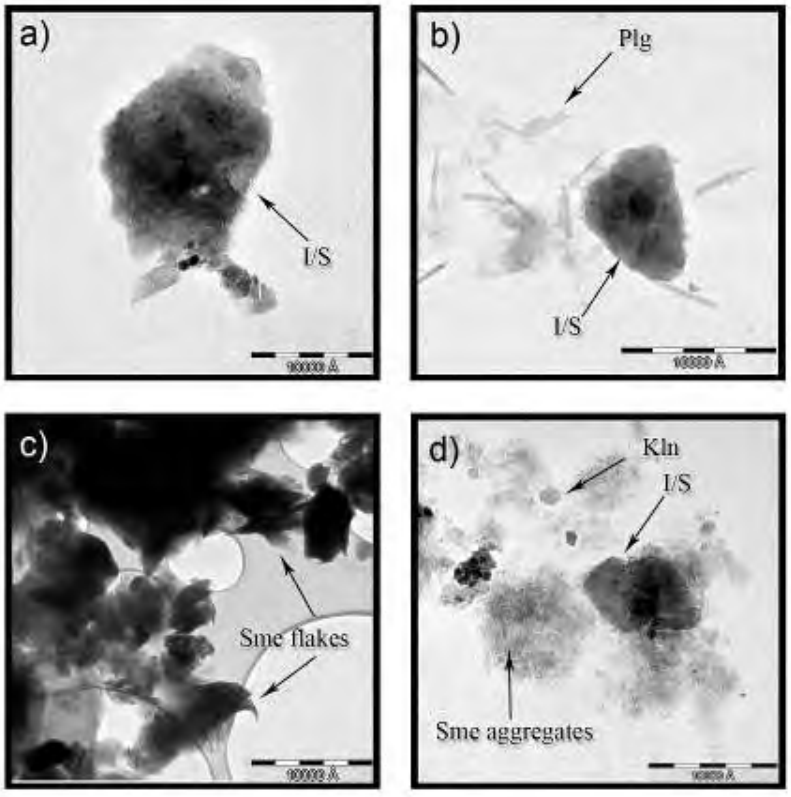

Fig. 3.-

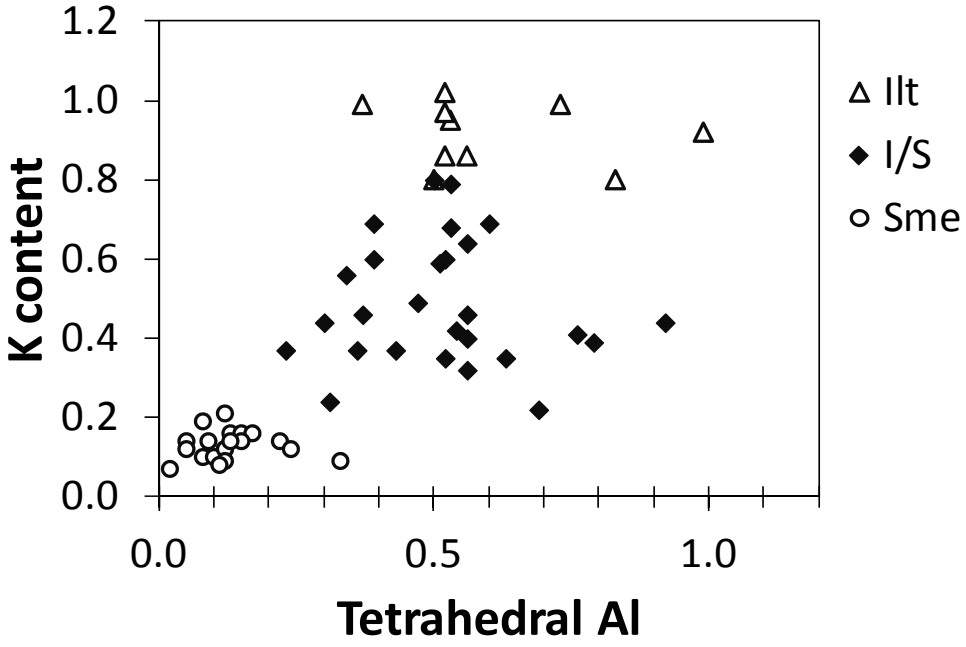

Fig. 4.-

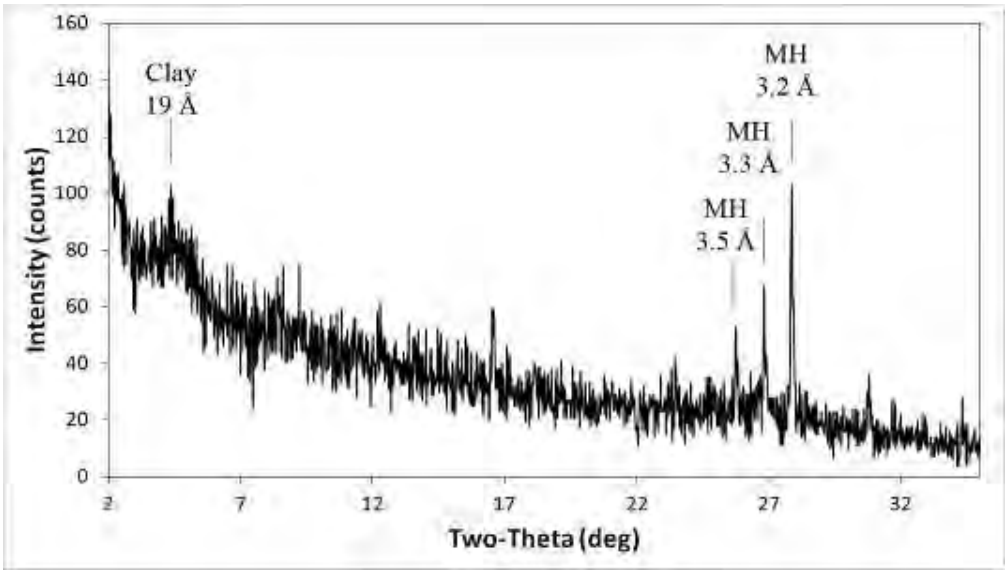

Fig. 5.-

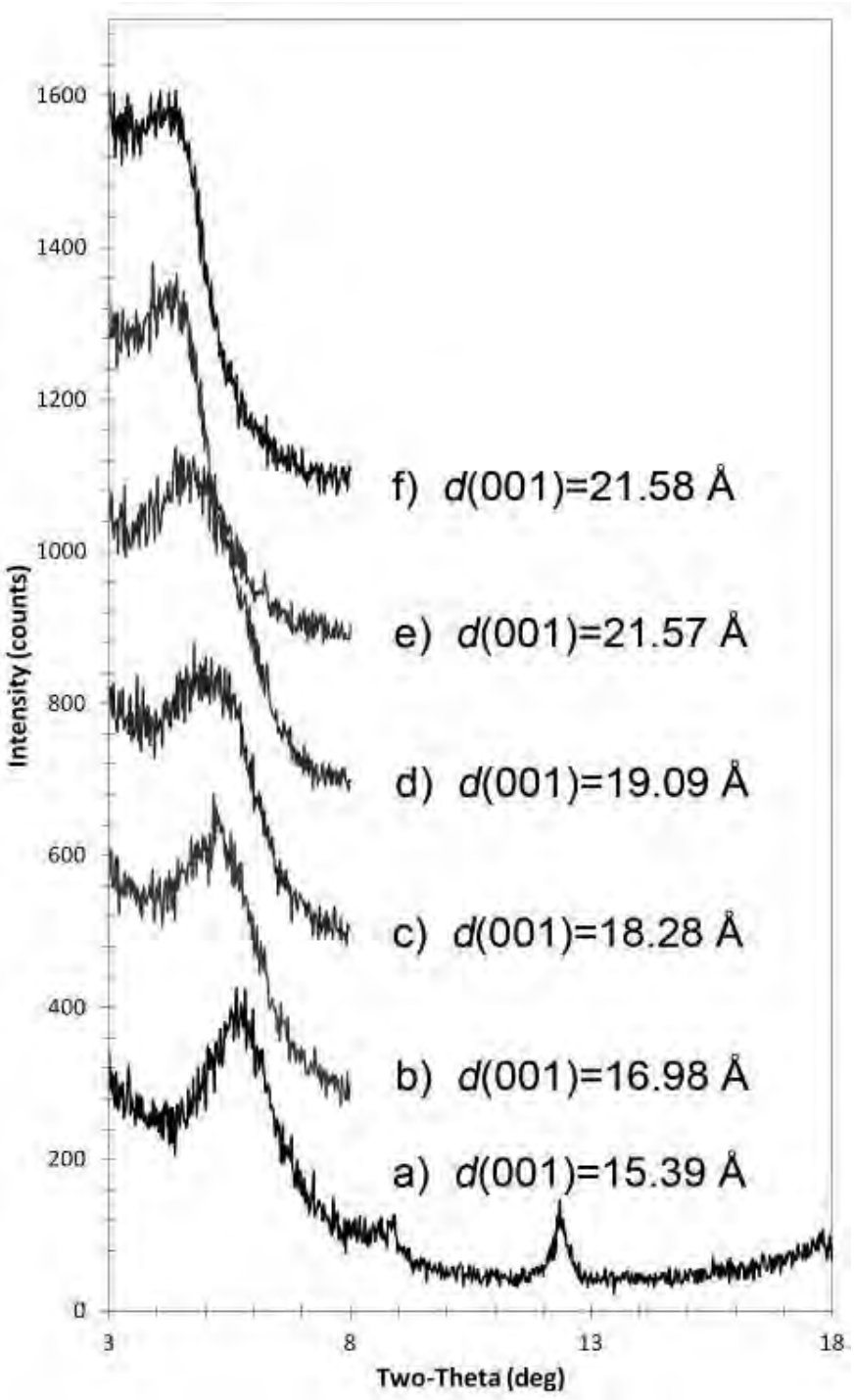

Fig. 6.-.

1072 a

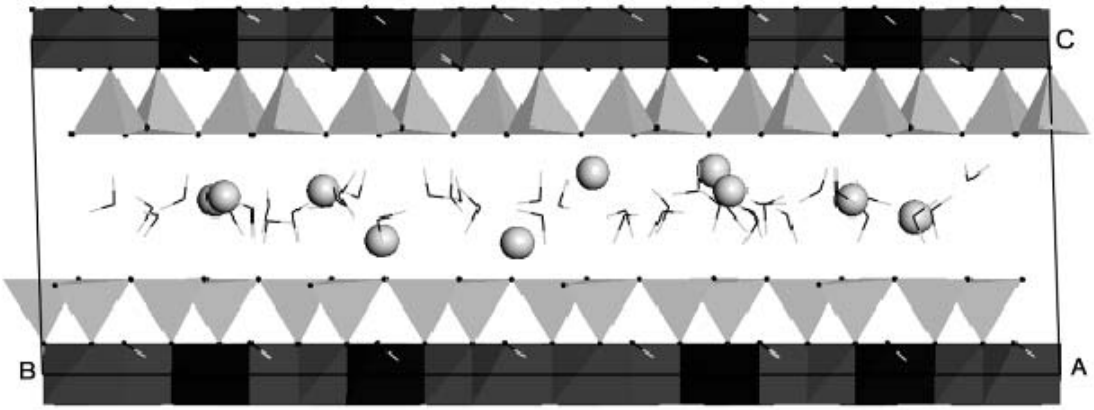

1073
1074 b

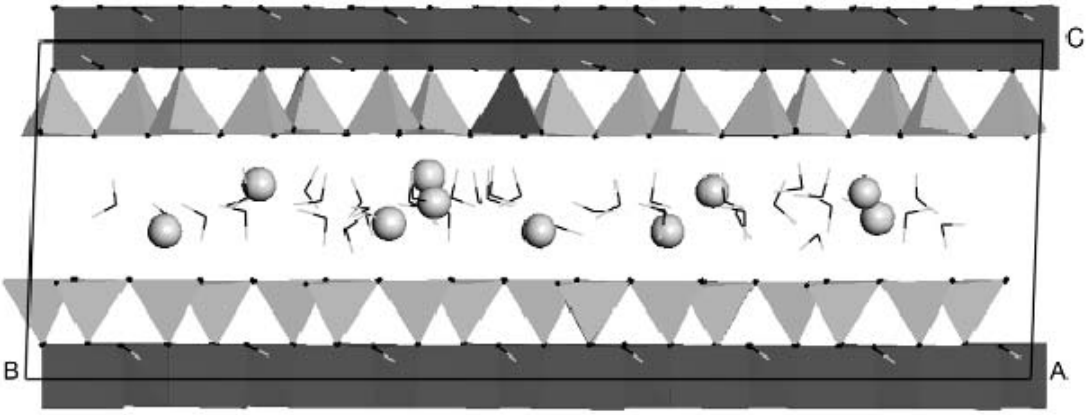

1075
1076 **Fig. 7.-**

1077

1078
1079

a

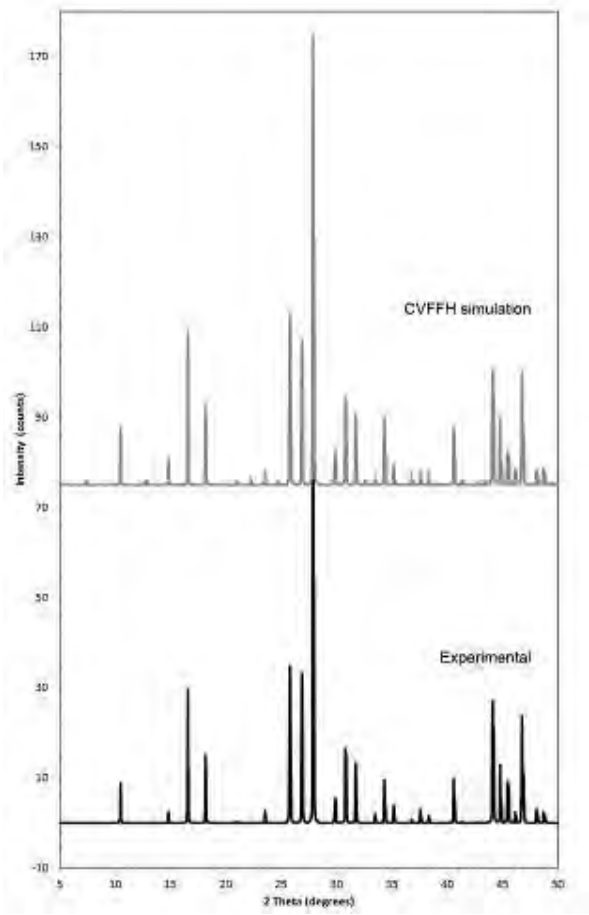

b

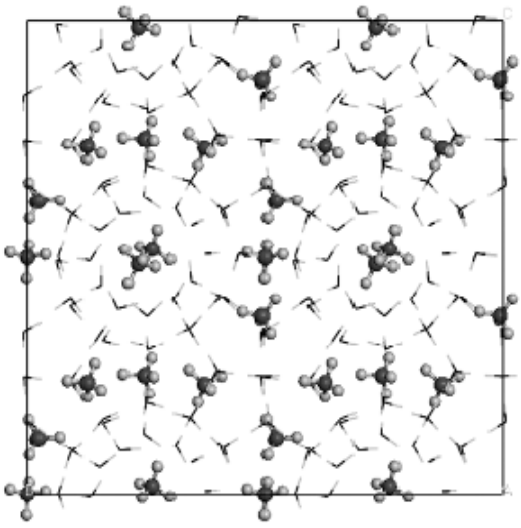

Fig. 8-.

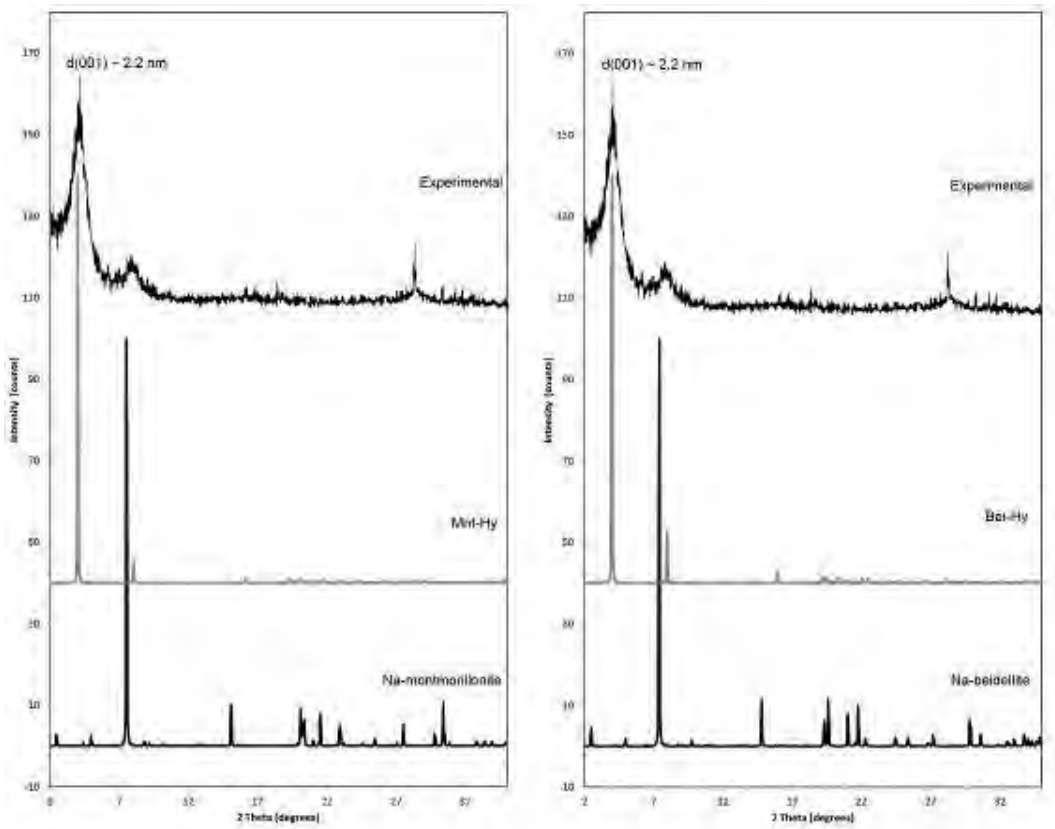

Fig. 9.-

1092

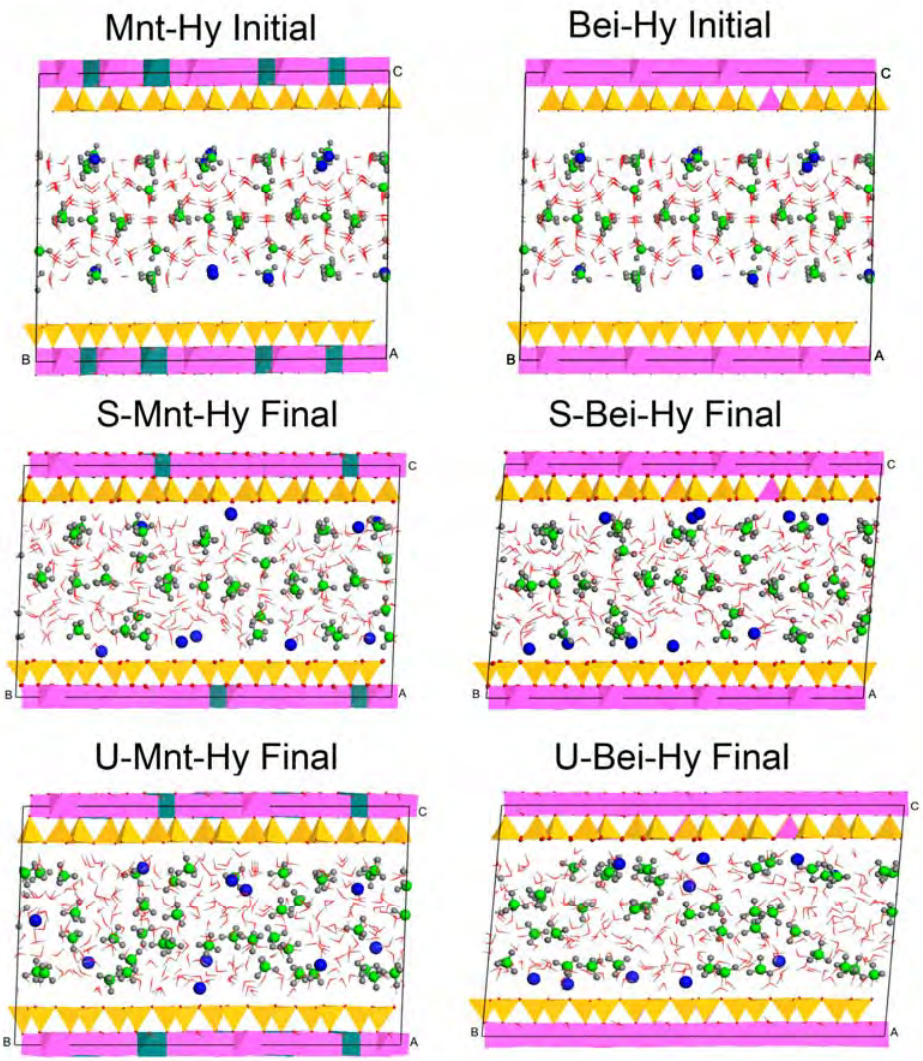

1093

1094 **Fig. 10.-**

1095 a

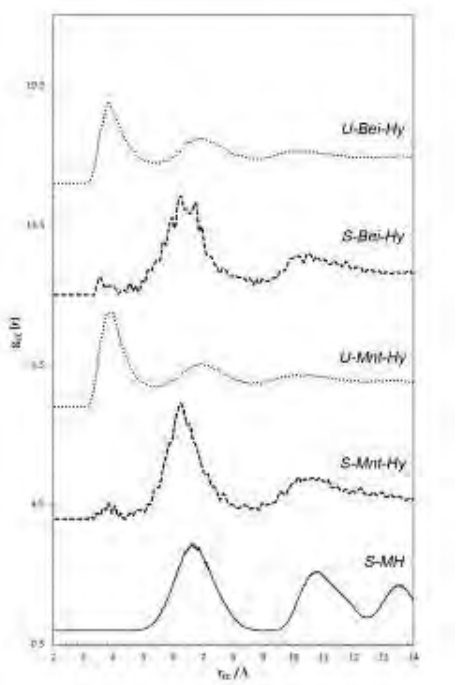

1096

1097 b

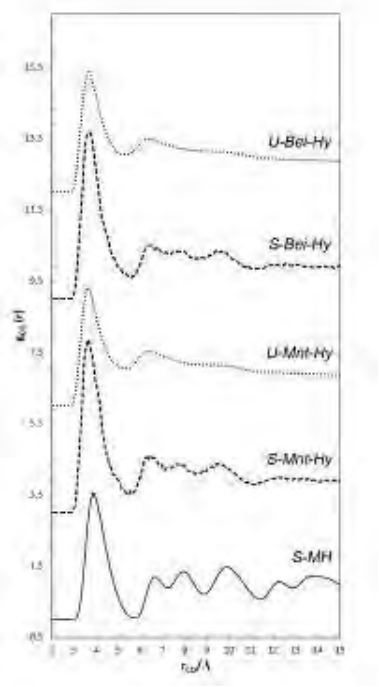

1098

1099 c

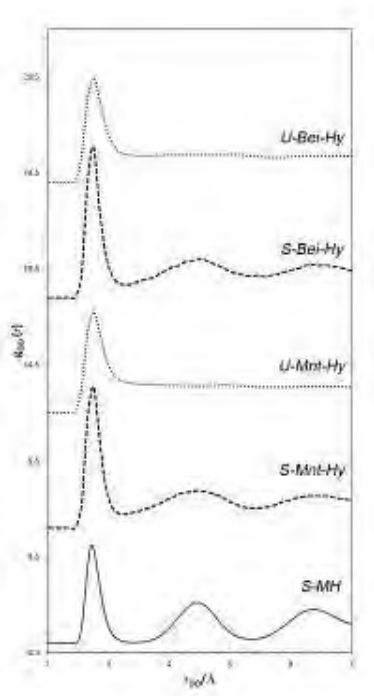

Fig. 11.-

1103

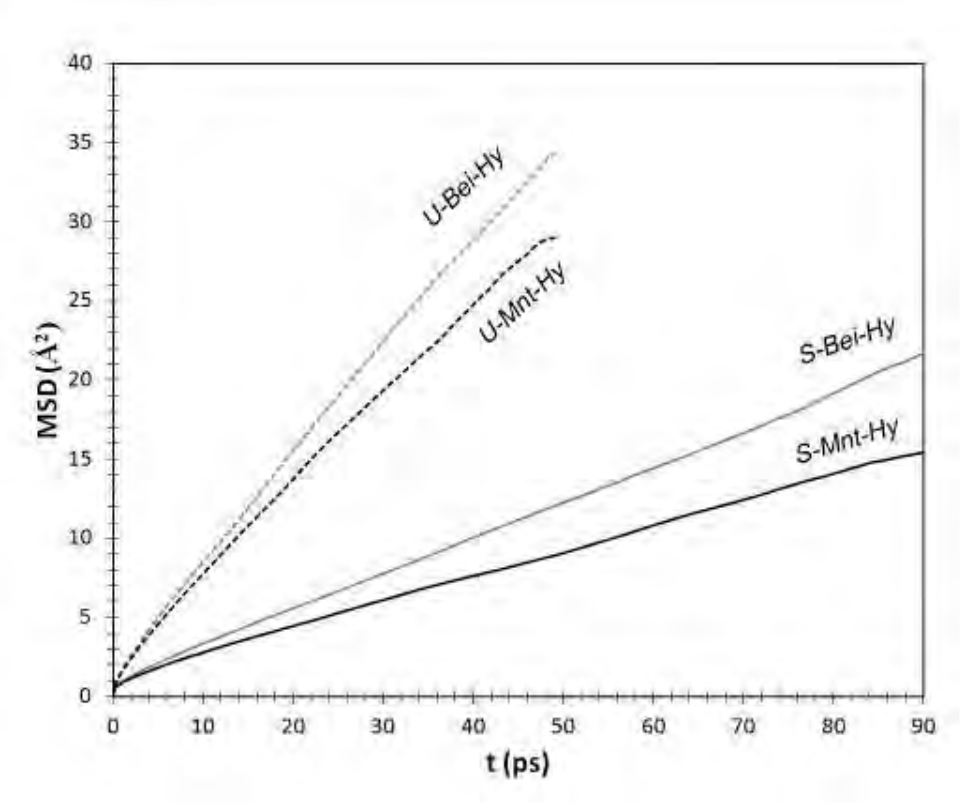

1104
1105 **Fig. 12.-**

1106

1107

1108 **Table 1.-** Structural formula of Interstratified I-S, smectites and illites normalized to
1109 $O_{10}(OH)_2$. ∑oct: sum of octahedral cations; ∑int: sum of interlayer charges.
1110

	Si	^{IV}Al	^{VI}Al	Fe	Mg	∑oct	K	Na	Ca	Mg	∑Int.
Interstratified I-S											
A2 -1	3.61	0.39	1.22	0.42	0.35	**2.00**	0.69	0.00	0.04	0.00	**0.76**
A2 -4	3.70	0.30	1.34	0.37	0.29	**2.00**	0.44	0.00	0.02	0.06	**0.60**
M3 -1	3.21	0.79	1.12	0.67	0.21	**2.00**	0.39	0.00	0.04	0.27	**1.01**
M3 -5	3.31	0.69	1.68	0.31	0.00	**2.00**	0.22	0.00	0.02	0.21	**0.68**
M3 -6	3.08	0.92	1.62	0.37	0.00	**2.00**	0.44	0.00	0.00	0.24	**0.66**
M3 -8	3.24	0.76	1.68	0.19	0.13	**2.00**	0.41	0.00	0.04	0.21	**0.91**
M3 -9	3.44	0.56	1.08	0.58	0.33	**2.00**	0.46	0.00	0.04	0.18	**0.90**
M3 -15	3.48	0.52	1.49	0.33	0.18	**2.00**	0.35	0.00	0.02	0.16	**0.71**
M3 -17	3.40	0.60	1.51	0.28	0.21	**2.00**	0.69	0.00	0.02	0.04	**0.81**
M4 -3	3.44	0.56	1.57	0.20	0.24	**2.00**	0.64	0.00	0.04	0.05	**0.82**
M4 -4	3.77	0.23	1.38	0.33	0.29	**2.00**	0.37	0.00	0.02	0.06	**0.53**
M4 -9	3.46	0.54	1.64	0.21	0.15	**2.00**	0.42	0.00	0.05	0.08	**0.68**
M4 -10	3.66	0.34	1.56	0.18	0.26	**2.00**	0.56	0.00	0.00	0.02	**0.60**
M4 -11	3.53	0.47	1.54	0.18	0.29	**2.00**	0.49	0.00	0.07	0.06	**0.75**
M4 -12	3.57	0.43	1.47	0.28	0.25	**2.00**	0.37	0.00	0.04	0.12	**0.69**
M4 -14	3.44	0.56	1.67	0.18	0.16	**2.00**	0.40	0.00	0.05	0.11	**0.72**
M8 -1	3.61	0.39	1.56	0.23	0.16	**2.00**	0.60	0.00	0.05	0.00	**0.70**
M8 -2	3.64	0.36	1.51	0.31	0.18	**2.00**	0.37	0.00	0.02	0.07	**0.55**
M8 -4	3.47	0.53	1.36	0.32	0.32	**2.00**	0.68	0.00	0.02	0.07	**0.86**
M8 -5	3.49	0.51	0.89	0.66	0.45	**2.00**	0.59	0.00	0.04	0.15	**0.97**
M8 -7	3.69	0.31	1.43	0.30	0.27	**2.00**	0.24	0.00	0.03	0.13	**0.56**
M8 -8	3.44	0.56	1.41	0.25	0.34	**2.00**	0.32	0.00	0.02	0.28	**0.92**
M8 -9	3.37	0.63	1.88	0.12	0.00	**2.00**	0.35	0.00	0.02	0.12	**0.63**
Smectites											
A2 -4	3.67	0.33	1.67	0.24	0.09	**2.00**	0.09	0.05	0.02	0.12	**0.42**
A2 -14	3.87	0.13	1.49	0.20	0.31	**2.00**	0.16	0.14	0.03	0.04	**0.44**
A2 -15	3.88	0.12	1.41	0.26	0.33	**2.00**	0.21	0.23	0.00	0.01	**0.46**
A2 -17	3.92	0.08	1.51	0.17	0.32	**2.00**	0.10	0.10	0.00	0.10	**0.40**
M3 -1	3.88	0.12	1.39	0.38	0.23	**2.00**	0.12	0.00	0.02	0.10	**0.36**
M3 -3	3.90	0.10	1.53	0.26	0.22	**2.00**	0.10	0.00	0.05	0.06	**0.32**
M3 -7	3.88	0.12	1.30	0.41	0.29	**2.00**	0.12	0.00	0.03	0.11	**0.40**
M3 -8	3.85	0.15	1.49	0.33	0.19	**2.00**	0.16	0.00	0.02	0.07	**0.34**
M4 -3	3.78	0.22	1.51	0.28	0.21	**2.00**	0.14	0.00	0.02	0.13	**0.42**
M4 -6	3.76	0.24	1.65	0.21	0.14	**2.00**	0.12	0.00	0.03	0.10	**0.38**
M4 -14	3.83	0.17	1.50	0.26	0.24	**2.00**	0.16	0.00	0.02	0.11	**0.42**
M4 -19	3.85	0.15	1.44	0.38	0.18	**2.00**	0.14	0.00	0.00	0.10	**0.34**
M8 -8	3.88	0.12	1.50	0.24	0.25	**2.00**	0.09	0.00	0.07	0.07	**0.37**
M8 -12	3.87	0.13	1.57	0.23	0.20	**2.00**	0.14	0.00	0.00	0.09	**0.32**
M8 -14	3.95	0.05	1.50	0.24	0.26	**2.00**	0.14	0.00	0.03	0.05	**0.30**
M8 -20	3.92	0.08	1.36	0.40	0.25	**2.00**	0.19	0.00	0.00	0.07	**0.33**
M12 -2	3.95	0.05	1.57	0.17	0.26	**2.00**	0.12	0.00	0.05	0.05	**0.32**
M12 -4	3.91	0.09	1.55	0.20	0.25	**2.00**	0.14	0.00	0.03	0.07	**0.34**
M12 -13	3.89	0.11	1.53	0.22	0.25	**2.00**	0.08	0.00	0.02	0.12	**0.36**
M12 -14	3.98	0.02	1.44	0.29	0.27	**2.00**	0.07	0.00	0.00	0.11	**0.29**

					Illites						
	A2 -2	3.48	0.52	1.43	0.25	0.27	**1.95**	0.86	0.00	0.04	0.00	**0.93**
	M3 -2	3.01	0.99	1.89	0.02	0.14	**2.05**	0.95	0.00	0.02	0.00	**0.99**
	M3 -7	3.17	0.83	1.32	0.38	0.40	**2.09**	0.92	0.00	0.02	0.00	**0.95**
	M4 -2	3.50	0.50	1.31	0.37	0.32	**2.01**	0.80	0.00	0.00	0.00	**0.80**
	M4 -3	3.27	0.73	1.63	0.20	0.23	**2.05**	0.80	0.00	0.00	0.00	**0.80**
	M4 -6	3.48	0.52	1.32	0.25	0.40	**1.97**	0.99	0.00	0.00	0.00	**1.03**

1111

Table 2.- Cell parameters and select interatomic spacings of Na-montmorillonite and Na-beidellite unit cells (distances in Å and angles in º).

Features	Exp[a]	Na-Mnt[b]	Mnt-Hy[c]	S-Mnt-Hy[d]	U-Mnt-Hy[e]	Na-Bei[f]	Bei-Hy[g]	S-Bei-Hy[h]	U-Bed-Hy[i]
a	5.18	5.16	5.41	5.41	5.42	5.16	5.42	5.42	5.43
b	8.95	8.95	8.91	8.92	8.93	8.92	8.92	8.92	8.93
c	12.34	12.08	23.15	23.18	23.19	12.34	22.94	22.97	22.98
d(001)	12.13	11.75	22.04	22.06	22.08	11.98	22.23	21.93	22.27
α	90.0	88.0	92.1	92.2	92.2	92.2	94.5	94.5	94.5
β	100.6	103.3	107.8	107.8	107.8	103.8	104.3	104.3	104.3
γ	90.0	90.1	89.3	89.4	89.3	89.4	89.4	89.4	89.4
d(Si-O)	1.65	1.66	1.65	1.65	1.65	1.67	1.65	1.65	1.65
d(Al-O)	1.94	1.94	1.95	1.95	1.95	1.94	1.95	1.95	1.95
d(O-H)		0.93	0.95	0.95	0.95	0.93	0.95	0.95	0.95
d(Na..O_{clay})		2.44	2.40	2.45	2.45	2.35	2.30	2.35	2.35
d(Na..O_w)		2.44	2.45	2.45	2.45	2.44	2.50	2.45	2.45
d(O_w..O_w)		2.74				2.73			

[a] Neutron Diffraction experimental data (Gournis et al., 2008); [b] Na-montmorillonite optimized at variable volume; [c] Montmorillonite-methane hydrate intercalate optimized at variable volume; [d] Montmorillonite-methane hydrate intercalate, averaged values from MD simulations at 273K and 40Bar;[e] Montmorillonite-methane hydrate intercalate, averaged values from MD simulations at 320K and 40Bar; [f] Na-beidellite optimized at variable volume; [g] Beidellite-methane hydrate intercalate optimized at variable volume; [h] Beidellite-methane hydrate intercalate, averaged values from MD simulations at 273K and 40Bar; [i] Beidellite-methane hydrate intercalate, averaged values from MD simulations at 320K and 40Bar;